CrossMark

ORIGINAL PAPER

Discrete modelling of rock avalanches: sensitivity to block and slope geometries

Guilhem Mollon[1] · Vincent Richefeu[2,3] · Pascal Villard[2,3] · Dominique Daudon[2,3]

Abstract A discrete element model was used to highlight the influence of size, aspect ratio and roundness of blocks onto the propagation of granular flows in order to obtain a more realistic modelling of rock avalanches. The numerical model accounts for energy dissipations by shocks and friction within the granular mass or at the base of the avalanche. A parametric numerical study was performed, based on laboratory experiments involving an assembly of small bricks. A particular attention was paid to explain how the block and slope geometry influence the kinematics of the avalanche (sliding or rotation of particles), and how the dissipative modes are modified (shocks or friction). In particular the effects of elongation, size and roundness of blocks combined to slope undulation were investigated. It was shown that these geometric aspects may have some complex implications in the mechanism of propagation of the granular flow and need to be taken into account to predict properly the final position of the deposit and the area impacted by individual blocks.

Keywords Rock avalanches · Discrete element modelling · Dissipative modes · Particle shape · Slope geometry

1 Introduction

Among the numerous natural hazards threatening human development in mountainous areas, rock avalanches are one of the less predictable. Depending on the site and conditions, such events may happen with various time–frequencies, and the range of possible implied rock volumes crosses several scales, running from a few hundred to several millions of cubic meters. Leaving aside the complicated topic of the triggering of rock avalanches (which may be related to several complex and interrelated events of diverse nature such as meteorological, geological, human, etc.), a strong uncertainty exists on the trajectory of such an avalanche and on its stopping area. This is regrettable, since such knowledge would improve our ability to prevent economic and/or human disasters by placing relevant countermeasures to rock avalanches, or most often, if their expected volume is too important, by simply avoiding human development in hazardous areas. To enhance the prediction of such hazardous areas, many authors have conducted experimental and numerical studies. Small-scale or medium scale laboratory experiments have been often used to investigate the influence of geometric characteristics such as the slope geometry, the shape or the size distribution of particles, onto the kinematics of granular flows, and the position and the shape of the deposits. Sand or gravel [2,8,13,15,20,26,27,48] are often used but cubiform granite blocks [35,48], rectangular bricks [26], glass beads or lens-like-shaped plastic particles [40] are also tested to catch the influence of the particle shapes onto the granular flow. The influence of the grains size and gradation of the granular material was also investigated. Cagnoli and Romano [2], conclude that the finer the grain size, the larger the mobility of the center of mass, while Goujon et al. [15] show on the base of experiments performed with bimodal mixtures of grains, that the large particles are found at the surface, at the lateral borders and at the front of the final deposit while the small particles are located preferentially at the base of the flow. Experimental works performed by Okura et al. [35] revealed that the runout distance had a

✉ Guilhem Mollon
guilhem.mollon@gmail.com

1 LaMCoS, CNRS UMR 5259, INSA Lyon, Université de Lyon, Campus LyonTech la Doua, Bâtiment Jean d'Alembert, 18/20 rue des Sciences, 69621 Villeurbanne Cedex, France

2 Université Grenoble Alpes, 3SR, 38000 Grenoble, France

3 CNRS, 3SR, 38000 Grenoble, France

positive correlation with the rockfall volume and that the relative positions of each block along the slope direction were not changed during rockfall movement. In the same way, flume tests performed by Yang et al. [48] show that the mass-front velocity increased with the volume for mono-materials while the velocity of a composite of cobbles and gravel with a large volume was almost the same as the mono-material of cobbles and of gravel with a small volume.

However, due to the experimental difficulty to perform measurements at the scale of the block within the avalanche, numerical models such as continuum approaches [25,29,36, 37] or discrete element models [1,3,6,21,35,43,45,47,50] are needed to get a better understanding of the mechanisms involved during the granular flows. The continuous models are usually based on the assumptions of fluid mechanics [25,29,36,37] and often take account of the whole dissipative phenomena via a dynamic friction coefficient acting at the base of the flow. These methods are simple to use but they remain difficult to apply to real cases since their parameters are necessarily obtained by back-analysis [20]. An alternative method used in rock mechanics is the Discontinuous Deformation Analysis (DDA, [42]), which is based on continuous methods used to solve for stress and deformations fields inside separate blocks, but accounts for the interaction of independent elements along discontinuities. Among the numerical methods, only the use of discrete models which take efficiently into account the interactions in the bulk of the granular material (collisions and friction) are able to give relevant information on the kinematics of each particle and on the mechanisms of energy dissipation occurring both at the base of the avalanche and within the granular mass [1,3,6,21,35,43,45,47,50]. Various strategies can be used to take account of the dissipative mechanisms at contact point such as viscous contact models [3], damping models [45] or specific dissipative contact laws as the one used for this study [1]. Compared to other discrete models based on the use of spheres or clumps made of spheres (useful to optimize the contact detection algorithm), the present model uses complex shaped elements to catch more realistic rebound behaviors.

Discrete-element models (DEMs) offer an interesting alternative to the continuous approaches in the sense that they reduce the amount of assumptions on the constitutive behavior of the granular material composing the flowing rock mass [22]. They also seem to be more representative for the modeling of certain classes of rock avalanches, which are too coarse to be regarded as a fluid and cannot be accurately modeled by continuous approaches. In the simplest DEM approaches, a granular mass is modeled by an assembly of rigid discs/spheres which interact by the means of a chosen contact law which controls the direction and norm of the frictional and repulsive forces that may exist during the contact between two particles [9,24]. These forces, together with the gravity, are then used to solve explicitly in time the

equations of motion applied to each particle. Several ways exist to improve such a simple modelling: using complex contact laws, accounting for interparticle cohesion, coupling with an interstitial fluid [10,16,38,41,49], or allowing the particles to break up [11,46], among others. These various techniques represent the state of the art in discrete modelling, and might soon be applied by the scientific community to the prediction of rock avalanches. Because of the inherent limitations of spheres (namely, their lack of resistance to rolling), another important trend is to use particles with more complex shapes to make the simulated granular mass more realistic from a geometric point of view [44], e.g. ellipsoids [23], polygons [7,12,19,28], polyhedra [5,14,17] and superquadrics [18,34]. Although some recent works [30–32] proposed to account for the whole complexity of the possible block shapes, it is easier to introduce some rather simple geometric shapes such as clusters of discs or spheres, ellipses or ellipsoids, polygons or polyhedrons, spheropolygons or spheropolyhedrons. This last technique is used in the present paper.

To test the ability of the discrete element (DE) approach to simulate granular flow and to predict position and shape of the deposit, Richefeu et al. [39] have numerically reproduced a laboratory experiment conducted by Manzella and Labiouze [26]. In their paper and in this one, the term "rock avalanche" is used to describe a large class of collective rock flows of very various magnitudes, in a more general way than in the classic literature on the topic. Their experiment (Fig. 1), referred to hereafter as the reference experiment, aimed at reproducing at small scale a rock avalanche with controlled conditions. It consisted in the launch, avalanche, and deposition of a granular mass along a planar slope having a sharp change of gradient. The upper slope was inclined at 45° while the lower slope was horizontal. Forty litres of small clay bricks, measuring $31 \times 15 \times 8$ mm, were randomly dropped into a rectangular box (dimensions $0.4 \times 0.2 \times 0.6$ m). This shape was chosen because of its simplicity, but also because it is sometimes observed in real events (Fig. 2, taken from Cuervo et al. [4]). Brick density was 1700 kg/m^3, and the apparent density of the packed bricks was 1000 kg/m^3. The box was positioned at a height of 1 m above the inclined plane, its lower face was opened and the material was released onto the slope. The velocity of the granular mass during the avalanche and the dimensions of the material deposit on the horizontal plane were measured using optical methods. In order to demonstrate the predictive ability of our DEM approaches, real rectangular shapes of the bricks were taken into account (this was done quite naturally in the spheropolyhedrons framework). Contact law parameters (brick/brick and brick/slope) were calibrated considering energy dissipations, based on additional experiments performed for this purpose, which consisted in the fall and bouncing of single particles filmed with high-speed cameras [39]. When
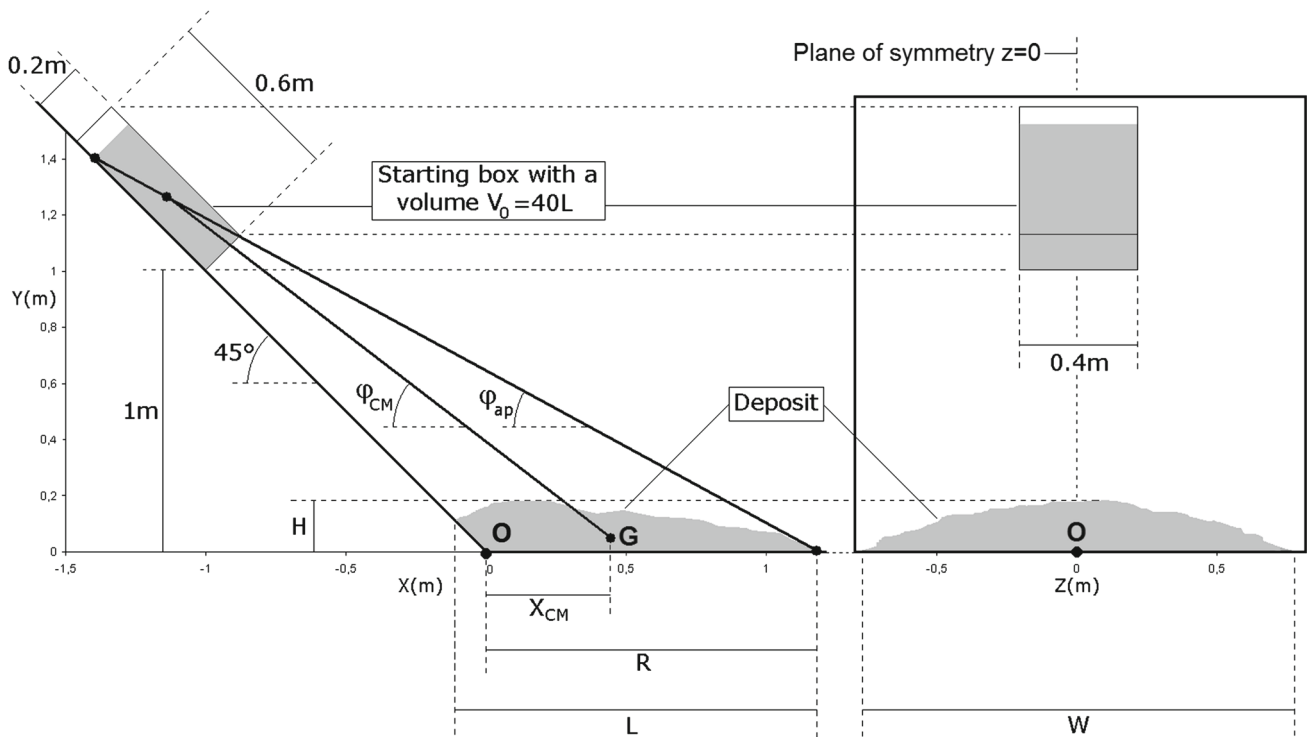
Fig. 1 Layout of the reference experiment reproduced in the present simulations, showing the length *L*, width *W*, thickness *H*, and runout length *R* of the deposit, the X-coordinate X_{CM} of its centre of mass, and the fahrböschung φ_{app} and travel angle φ_{CM} of the avalanche (partially taken from Richefeu et al. [39])

Fig. 2 Examples of somewhat rectangular blocks observed in a rock-fall near Millau, France (from Cuervo et al. [4])

compared to the experimental results, the final simulation provided satisfactory outputs in terms of avalanche kinematics, and deposit size, shape and location. This result was particularly interesting because it proved that DEM may be predictive without the need to run any back-analysis on a full event to calibrate the contact law and the particles geometry.

To better grasp the physical mechanisms involved during granular flows, a parametric study on the contact parameters, on the slope angle, and on the geometric properties of the

support was performed in Mollon et al. [33]. It was observed that the use of a surface roughness (composed of asperities with a size close to that of the typical grain of the avalanche) could trigger a change in a flow regime. In the present paper, we provide a detailed analysis of this phenomenon, and we complete the parametric study by focusing on block geometry, namely their size, aspect ratio and roundness.

2 Description of the simulations and of the post-processing

2.1 Simulations

The geometry of the simulations described hereafter is identical to that already presented in Richefeu et al. [39] and Mollon et al. [33], and reproduces the actual geometry of the reference experiment described in Manzella and Labiouse [26]. To prepare the virtual granular sample, the bricks are placed on a regular lattice (sparse enough to avoid interpenetration) and randomly oriented. They are then packed under gravity in a virtual vertical box, the desired solid fraction (identical to the experimental one) being obtained by calibrating the interparticle friction coefficient by trials and errors. Before releasing the mass, the friction coefficient is set

to the desired value and the box is inclined at 45° and placed at the proper height on the virtual slope. The lower wall of the box is removed at $t = 0$, triggering the granular flow along the slope, which occurs until all the mass has stopped around the zone of transition with the horizontal plane.

To simulate properly the interactions between the bodies involved in the system (bricks and slope), a contact law has been chosen in Richefeu et al. [39]. This contact law accounts for a normal and a tangential linear stiffnesses (respectively k_n and k_t) which allow to develop repulsive normal and tangential forces in case of interpenetration between two solids. Besides, energy dissipations are accounted for in the case of friction (in the tangential direction, using a classical Coulomb friction with a coefficient μ^*) and of collision (using a coefficient of restitution e_n^2, introduced by the mean of a ratio between the loading and unloading stiffnesses in the normal direction). No viscous effect is accounted for in this contact model. The numerical contact parameters, summarized in Table 1, are identical to those calibrated experimentally in Richefeu et al. [39]. For these calibrations, additional experiments involving bouncing of single particles were performed and reproduced numerically, and the parameters so-obtained were further introduced in a full simulation of the avalanche experiment. The good quantitative prediction of the experimental avalanche by the simulation provided evidence that the contact model is reliable. It also proved [39] that DEM

is able to predict the collective behavior of granular masses after calibration on individual behaviors, without the need to perform a back-analysis of a full event.

In this study, the particles composing the granular material differ from the original ones (i.e. from the ones used in the Manzella and Labiouse [26] experiments and reproduced in our previous work). Nine different types of particles, referred to as letters from A to I, are used in the present paper. Geometrical properties of these particles are provided in Fig. 3. On one hand, particles A to E are identical in proportions to the original ones, except that a homothetic factor was applied to their dimensions. Particles C are actually identical to the original rectangular ones, while A and B are smaller and D and E are bigger. On the other hand particles F to I explore different shapes. Particle F is a perfect cube with a volume similar to the one of the original rectangular particles, and particles G to I are obtained from particle F by "cutting" its corners and altering its angularity. This alteration is controlled by a cutting parameter c, which runs from 0 (unaltered cube, case F) to roughly three-quarters of a half-length of the initial cube ($c = 4$ mm, case I). In all cases, the number of particles packed in the starting box is chosen in order to reproduce both the apparent volume and the bulk density of the granular packing of the reference experiment. Thus, for each one of these nine packings, the unit weight of the material composing the blocks is equal to 17 KN/m³, the total granular mass is roughly 40 kg, and the apparent volume is roughly 40 l. As a consequence, this paper will not investigate the scale effects related to the total volume of the material composing the avalanche, but only those related to its granular content. In the case of the largest bricks (case E), the total number of blocks is equal to 790 and the typical thickness of the avalanche is close to twice the length of the brick. In contrast, in the case of the smallest bricks (case A), about

Table 1 Parameters of the contact laws

	e_n^2	μ^*	k_n (N/m)	k_t/k_n
Brick–Slope contact (BS)	0.53	0.46	100,000	0.42
Brick–Brick contact (BB)	0.13	0.86	100,000	0.27

e_n^2 is the coefficient of restitution, μ^* is the coefficient of friction, k_n and k_t are the normal and tangential stiffnesses

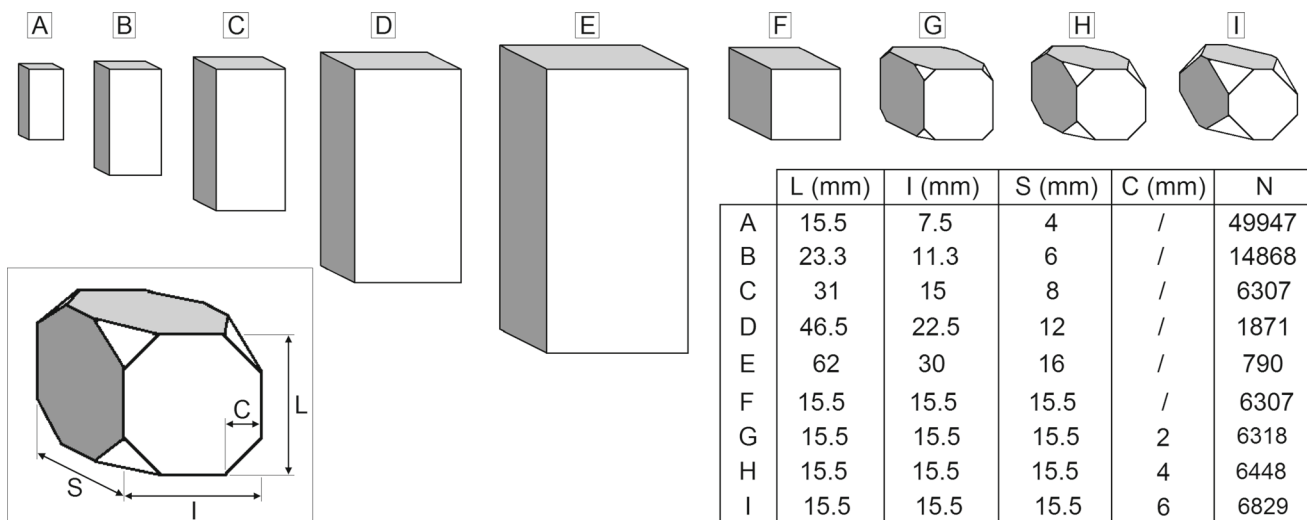|	L (mm)	l (mm)	S (mm)	C (mm)	N
A	15.5	7.5	4	/	49947
B	23.3	11.3	6	/	14868
C	31	15	8	/	6307
D	46.5	22.5	12	/	1871
E	62	30	16	/	790
F	15.5	15.5	15.5	/	6307
G	15.5	15.5	15.5	2	6318
H	15.5	15.5	15.5	4	6448
I	15.5	15.5	15.5	6	6829

Fig. 3 Overview of the nine considered particles with their maximum (*L*), intermediate (*l*), and minimum (*S*) dimensions, their corner-cutting parameter (*c*, identical in the three directions of space), and the total number (*N*) of particles composing the avalanche
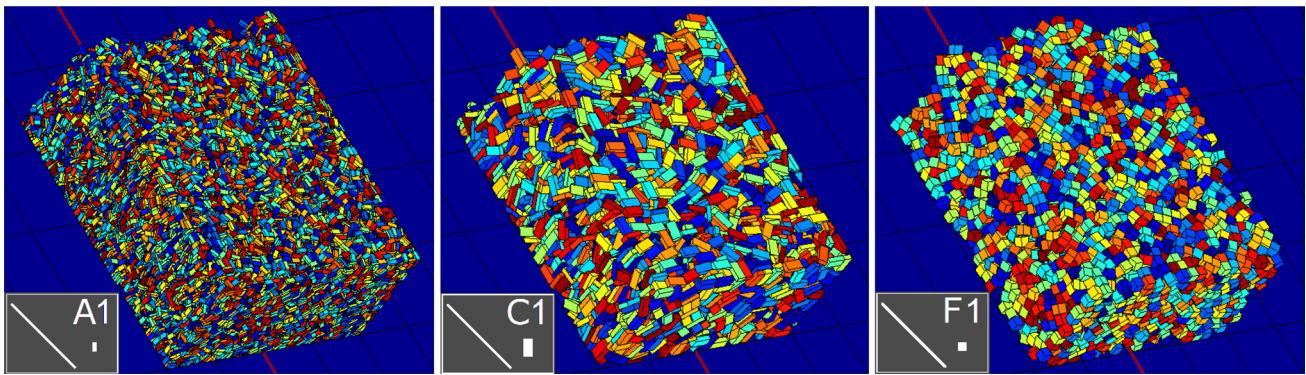
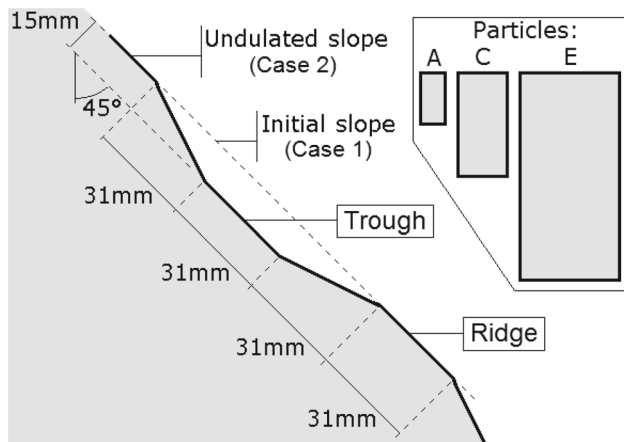**Fig. 4** Initial packings for particles *A*, *C*, and *F*

Fig. 5 Dimensions of the undulations of slope 2, and scaled front-views of some typical particles used in the study

50,000 blocks are considered and the typical thickness of the avalanche is close to eight times the length of the brick. Some illustrative initial packings are provided in Fig. 4.

In addition to the size and shape of the bricks, this paper also pays attention to the role of the slope geometry. For this purpose, two cases are considered. In case 1 the slope is perfectly planar and smooth, and its geometry and coefficient of friction (0.46) are identical to those of the reference experiment. In case 2, an additional waviness is introduced in the form of sharp ripples. As shown in Fig. 5, these undulations are scaled to the dimensions of the original rectangular bricks. Indeed, the length of the planar zone of each trough and each ridge is equal to the length of bricks C (31 mm) and the depth of the undulation is equal to the intermediate dimension of bricks C (15 mm), in such a manner that a brick of type C may exactly lie in a typical trough. Hence, the bricks A and B are smaller than the typical size of the undulation while bricks D and E are larger (they are unable to entirely reach the bottom of a trough). Due to their shapes, cubic or corner-cut particles F to I are also smaller than the undulation typical length. This case 2 is referred to as undu-

lated slope hereafter. Hence, the remainder of this paper will describe the numerical results obtained after running 18 simulations, which will be referred to as the index of the brick (A to I) followed by the index of the slope (1 or 2); e.g. B1 or G2. Specific interest will be paid successively to (1) the kinematics of the avalanche, (2) the sources and amount of energy dissipations, and (3) the position, size and shape of the granular deposit.

2.2 Post-processing methodology

Considering the kinematics of the avalanche, the most interesting quantities are the velocities and angular velocities of each brick, and the local values of the solid fraction of the granular assembly. This solid fraction is computed in the manner described in Mollon et al. [33]. For each particle i we wish to define a domain representing its closest neighborhood, and we first consider the N particles closest to i. Besides, for this measurement to remain local when applied to particles close to the external outline of the granular mass (i.e. with a limited number of close neighbors), we consider a sphere of radius d around the particle i, and discard the particles outside of this sphere. We then consider the $N' \leq N$ remaining particles and define a representative zone, determined by applying a close non-convex hull algorithm to the $N' + 1$ particles (including the particle i), dividing the total volume of these $N' + 1$ particles by the volume of the hull. The solid fraction so-obtained is assigned to the particle i, although it characterizes not only the particle but its close neighborhood. In the present paper, we use $N = 100$ and d equal to five times the intermediate dimension of the brick, which appears to be a good compromise and to provide meaningful and smooth results for display. One should note, however, that the notion of solid fraction is less relevant when applied to a small sample, since most of the blocks of such a sample are very close to its border. Hence, the solid fractions proposed hereafter for cases D and E are to be considered with caution.

The post-processing of energy dissipations is also identical to that proposed in Mollon et al. [33], and focuses on the time and space localization of the different sources of dissipations induced by the chosen contact law. There are four kinds of such a dissipation: it may be either frictional or collisional, and it may occur either at a brick–slope contact or at a brick–brick contact. At the end of the motion, the sum of the four cumulative terms of energy dissipation balances exactly the loss of potential energy induced by the avalanche. Since the total mass of material and the loss of elevation of the centre of mass are similar in all the simulations, the cumulative dissipated energy does not vary very much from one simulation to the other. However, the sources and locations of dissipations may be affected quite a lot by the parameters that are varied in the different simulations.

Considering a given granular deposit, there is no immediate way to provide its exact and meaningful dimensions since it is an assembly of individual solids. In the present study, these dimensions are computed using the non-convex enveloping algorithm described in details in Mollon et al. [33], which makes it possible to evaluate some relevant and reproducible boundaries of a cloud of points based on a density criterion. The quantities of interest characterizing the geometry of a deposit are provided in Fig. 1: the travel angle φ_{CM} (based on the centre of mass), the "fahrböschung" angle φ_{ap} (common terminology in the field of rock avalanches to define an apparent travel angle, computed based on the extreme points of the initial packing and of the deposit, see Fig. 1), the runout distance R (computed with respect to the point of change of slope gradient), the deposit length L, width W, and thickness H. In addition to these six classical parameters which describe the position and size of the main part of the deposit, we also study two additional quantities which are related to the blocks which get separated from the main deposit, and which may have some important consequences in the framework of a real rock avalanche. The first of these two parameters is called "1 % fractile in length", and is the distance from the point O intersecting the change of slope (Z axis) and the symmetry plane of the system (i.e. the plane $Z = 0$, see Fig. 1) above which only 1 % of the total amount of particles are found in the runout direction. For example, if this quantity is equal to 1 m, it means that exactly 1 % of the particles composing the initial packing have a runout distance longer than 1 m. Hence, it describes the axial dispersion of the final positions of the blocks. The second quantity is called "1 % fractile in width", and is analogous to the previous one except that it describes the transversal dispersion of the blocks and that it is measured with respect to the vertical plane of symmetry of the starting box (i.e. the plane $Z = 0$). For example, if this quantity is equal to 1 m, it means that exactly 1 % of the particles composing the initial packing finally stopped at a position located at more than 1 m from the plane of symmetry, either on a side or the other.

Section 3 will be dedicated to the sensitivity of the avalanche to the size of the blocks, and will thus focus on simulations A1 to E1 and A2 to E2. Section 4 will pay interest to the influence of the geometric proportions of the blocks (comparing particles A and F on both slopes 1 and 2), and Sect. 5 will be dedicated to their angularity (focusing on simulations F1 to I1 and F2 to I2).

3 Influence of the size of blocks

3.1 Avalanche kinematics

To study the kinematics of the avalanche, it is chosen here to focus on snapshots of the simulations A1, E1, A2 and E2 (i.e. smallest and largest brick sizes, on planar and undulated slopes). A meaningful comparison between the four cases is obtained by considering for each simulation a snapshot at the instant for which the front of the avalanche reaches the abscissa 0.4 m. Then, a number of transverse cross-sections (from −0.9 to 0.2 m, every 0.1 m, in vertical planes) are performed in order to get an insight of the avalanche, as well as a longitudinal cross-section in the plane of symmetry of the starting box ($Z = 0$ m). The results are plotted in Figs. 6, 7 and 8, for the velocities, the angular velocities, and the solid fractions respectively.

Figure 6 focuses on the velocity fields for the four simulations. A comparison between the cases A1 and E1 shows that the velocity profiles are very similar, exhibiting almost homogeneous velocities in vertical cross sections, with a regular acceleration all along the slope and a rapid deceleration around the zone of gradient change. The only minor difference between the two cases is the fact that the small bricks tend to exhibit more lateral spreading during the avalanche, while the large bricks remain more concentrated in the central area. This observation is valid down to the final deposit.

The velocity profiles obtained with an undulated slope are very different. In the case of small bricks (case A2), a very clear vertical gradient of velocity appears on the longitudinal cross-section, with interesting velocity patterns exhibiting the same periodicity than the waviness. The upper layer of the granular mass has a much larger velocity than the lower one, which is submitted to periodical cycles of acceleration–deceleration depending on the local value of the slope gradient. The transverse cross-sections show that this sheared flow is rather homogeneous in the entire width of the granular mass, since the velocity magnitude is almost independent from the elevation. This stratified flow is not observed in the simulation E2. Indeed, in the case of large bricks, there is no lower layer with very limited velocity like in the case of small bricks, and there is no identifiable velocity profile in any transverse cross-section. Instead of that, one
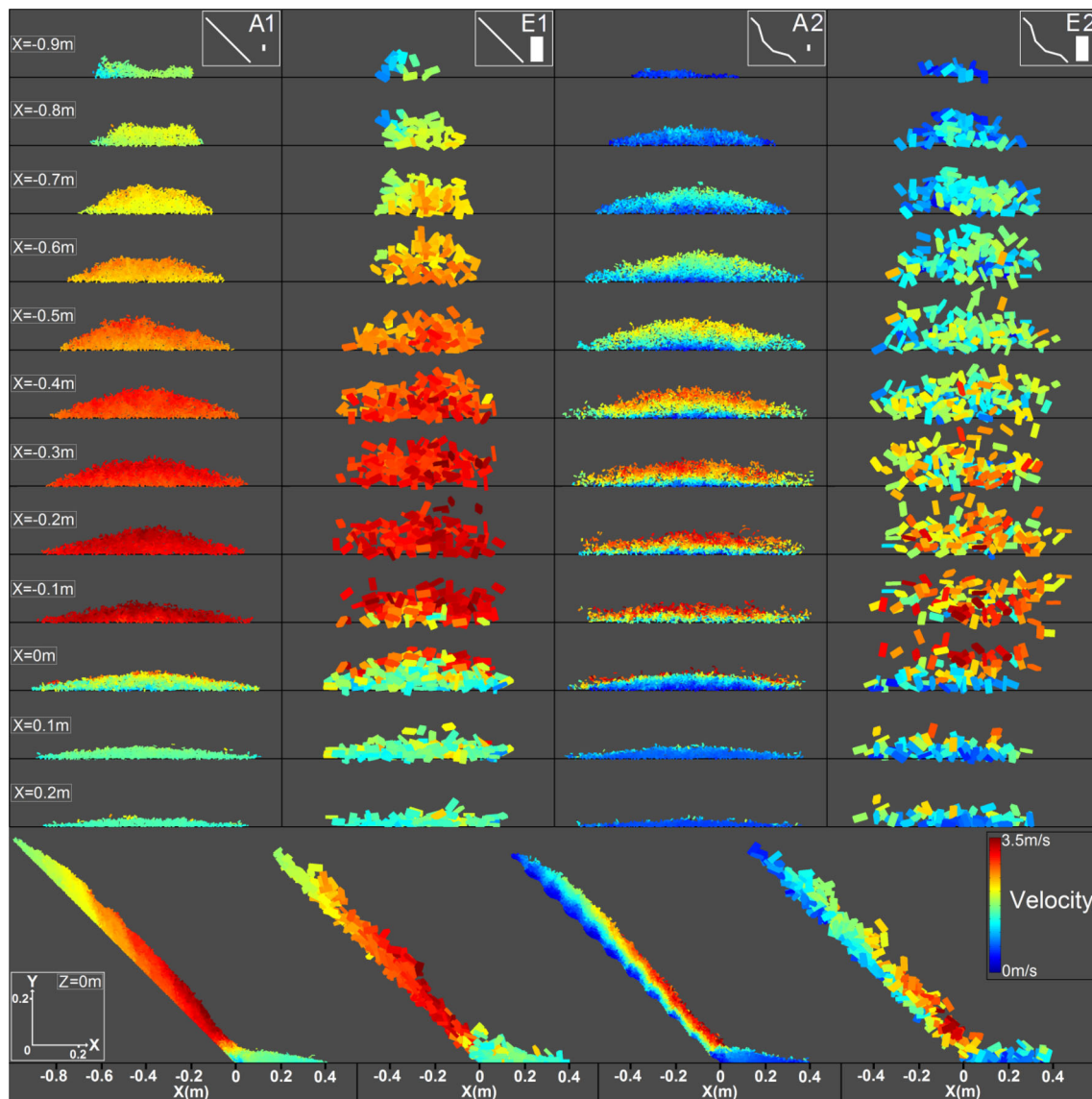
Fig. 6 Velocities of the particles for simulations *A1*, *E1*, *A2*, and *E2*, when the fronts of the avalanches reach X = 0.4 m. *Upper part* vertical transverse cross-sections at various abscises X; *lower part* longitudinal cross section in the plane of symmetry of the starting box

may observe a rather unstructured flow with very different velocities from a brick to the other.

The magnitudes of the angular velocities of each brick are plotted in Fig. 7 for the four simulations. The case A1 shows a limited amount of rotations among the particles, except in the area of gradient change, where the flow is strongly disturbed. Rotations are even smaller in case E1, and the disturbance in the transition zone seems less intense for large bricks. Overall, for the two cases A1 and E1, the avalanche is mostly in a translational motion (slipping regime), with homogeneous velocities and limited rotations. In contrast, large particle rotations occur in the case of a stepped slope, and rotations are more intense for the small blocks. The transverse cross-sections of simulation A2 show that the rotations

are homogeneous in the width of the avalanche, but exhibit some patterns along the vertical direction. This is confirmed by the longitudinal cross-section, which shows periodic patterns of large rotations alternating with zones of more calm flow, related to the wavelength of the undulations of the slope. Such patterns do not exist in the simulation E2, for which the brick rotations are rather important but unstructured.

Figure 8 presents the results in terms of local solid fraction. For the cases A1 and E1 on a planar slope, the density of the granular packing is rather homogeneous in the entire avalanche (except on its lateral edges), but the avalanche of small particles seems denser (solid fraction of about 0.35) than the one of large particles (solid fraction of about 0.25). The case E2 (large bricks on an undulated slope) also leads
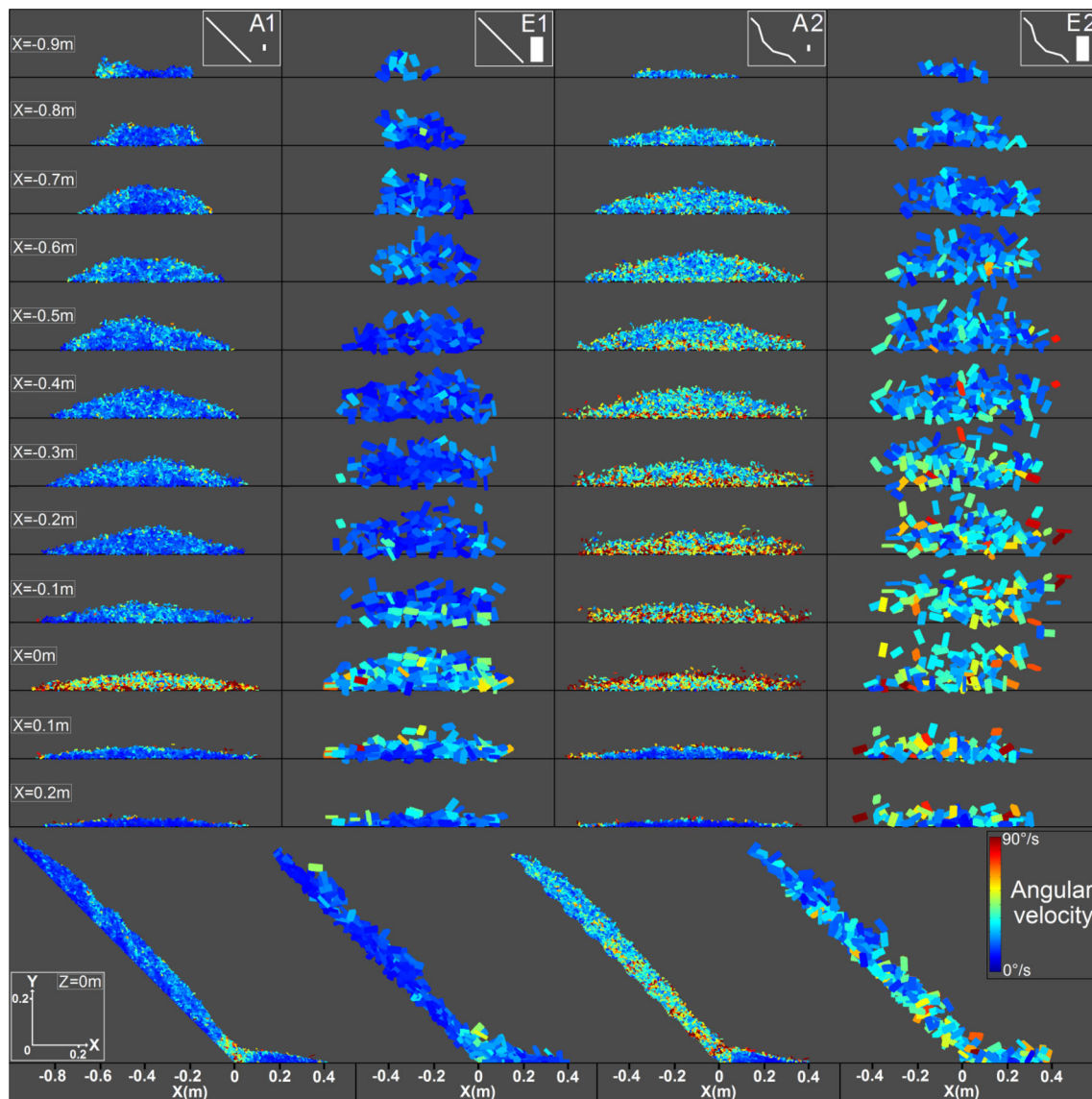
Fig. 7 Angular velocities of the particles for simulations *A1*, *E1*, *A2*, and *E2*, when the fronts of the avalanches reach X = 0.4 m. *Upper part* vertical transverse cross-sections at various abscises X; *lower part* longitudinal cross section in the plane of symmetry of the starting box

to a rather homogeneous density, but the granular packing in this case is very loose, with an average solid fraction of the order of 0.13. Combined with the observations of Figs. 6 and 7 (very heterogeneous values of the velocities and angular velocities from a particle to its neighbors), we may conclude that the flow regime is probably very collisional. The case A2 (small bricks on an undulated slope) is the only one for which there is a heterogeneous distribution of the solid fraction. In this simulation, there are interesting periodic patterns of density which follow the undulations of the slope, with zones of rather high densities (solid fraction close to 0.32) in the troughs of the slope and low densities (solid fraction of roughly 0.25) on the ridges. These density patterns are spatially synchronized with the ones observed in the velocity

field (Fig. 6), and the areas of high density are well correlated with the ones of low velocity. The transverse cross-sections of simulation A2 in Fig. 8 also show that the density is not homogeneous in the width of the avalanche: the packing is globally denser in the central part than in the lateral parts, although some other fluctuations add more complexity to this trend.

3.2 Energy dissipations

In Fig. 9, one may observe the repartition of the energy dissipations among different sources and locations, for the simulations A1 to E1 (planar slope) and A2 to E2 (undulated slope). This repartition is expressed in terms of percentage
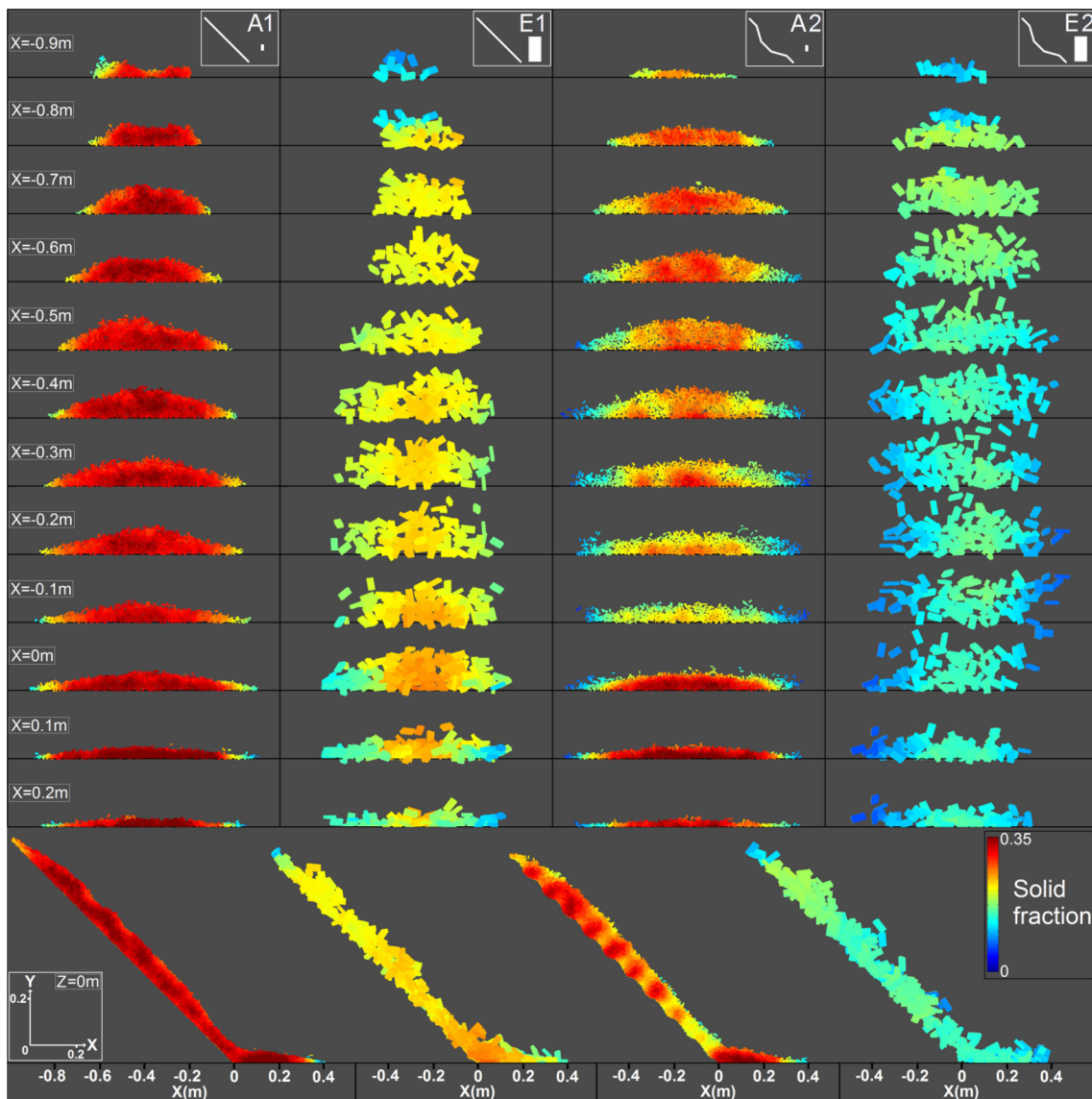
Fig. 8 Local solid fractions for simulations *A1*, *E1*, *A2*, and *E2*, when the fronts of the avalanches reach X = 0.4 m. *Upper part* vertical transverse cross-sections at various abscises X; *lower part* longitudinal cross section in the plane of symmetry of the starting box

of the total dissipated energy. The total cumulative dissipation is equal to the total loss of potential energy due to the avalanche, and is rather constant in all the simulations since the total mass of particles and the initial and final altitudes of the centre of mass of the granular matter are nearly constant. The four kinds of energy dissipations that are presented in this figure are related to the two dissipation mechanisms embedded in the chosen contact law (collisional and frictional dissipations, see Richefeu et al. [39] for more details), occurring either at a brick–brick contact or at a brick–slope contact. In order to investigate the location of the energy dissipations, three geometric zones are defined in Fig. 9: zone 1 corresponds to the slope, zone 3 corresponds to the horizontal plane, and zone 2 extends across the change of gradient

at the slope foot, also called transition zone. The sum of these twelve terms (two types of dissipations at two types of contacts and in three geometric zones) equals the entire dissipated energy, which is rather constant in the different simulations as explained above.

For all the bricks sizes, a quick comparison between the planar and the undulated slope shows the major differences between the two cases, and provides some energetic justifications to the kinematic observations made in the previous section. On the planar slope, the majority of the energy is dissipated by friction, mostly between the bricks and the support, which means that the avalanche is mostly in a slipping regime. Only a small fraction of the dissipation occurs by collisions, and this dissipation is concentrated in the transi-
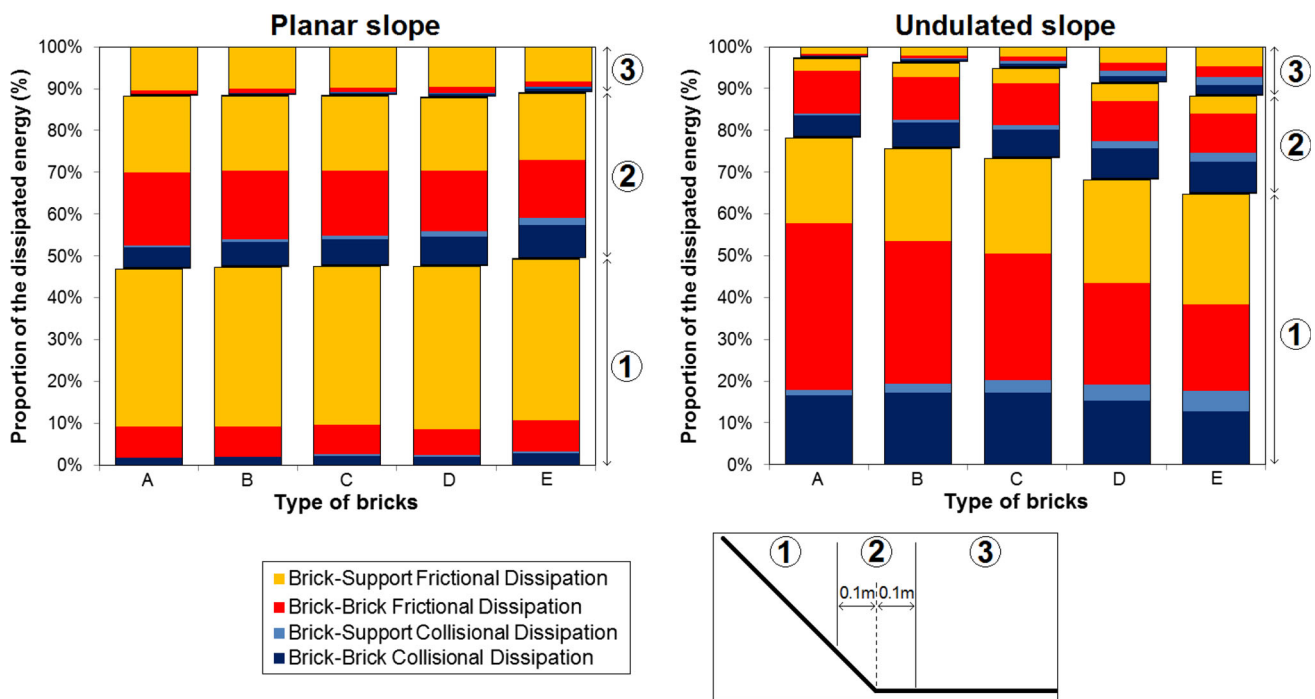
Fig. 9 Type and localization of the cumulative energy dissipations for various block sizes, on a planar and an undulated slope

tion zone for which the flow is disturbed by the change of gradient. After the transition zone, about 10 % of the energy remains to be dissipated in the zone 3 (i.e. on the horizontal plane). Overall, the influence of the size of the bricks on the modes and localizations of the dissipations seems very limited.

In contrast, for an undulated slope, the contribution of the brick–slope friction to the dissipation becomes minor, and the interparticle friction and the collisional dissipations become more significant. Besides, the size of the bricks seems to have a noticeable influence on the dissipation patterns: in case of small bricks, less than 3 % of the energy remains to be dissipated in zone 3, while this proportion reaches 10 % for large bricks. It appears that a large part of this difference is related to the friction between bricks in the zone 1 (i.e. on the slope), which is much more important in the case of small bricks (about 40 % of the total dissipation) than in the case of large bricks (about 20 % of the total dissipation). Increasing the size of the bricks also leads to an increase of the dissipations related to collisions on the support, which is consistent with the kinematic observations of the previous section (collisional flow in simulation E2).

These observations are further confirmed by Fig. 10 that provides the cumulative values of each type of dissipation as a function of time, for the simulations A1 to E1 and A2 to E2. In all the charts of this figure, the blue arrow points from the smaller bricks (case A) to the larger bricks (case E). The size of bricks induces some trends which are almost

the same on a planar and an undulated slope: considering larger bricks increases the collisional dissipations (either between the bricks or with the support), and decreases the frictional dissipations (except the brick–slope frictional dissipations on planar slope, which remain almost constant). Hence, whatever the type of slope, larger bricks lead to a more collisional flow while smaller bricks lead to an increase of the internal shear of the material. However, the quantitative influence of the bricks size is much less important on a planar slope than on an undulated slope. In the latter case, the use of small bricks strongly reduces the basal frictional and collisional dissipations, and operates a strong transfer to the frictional dissipation in the bulk of the avalanche. This is in good agreement with the kinematic observations (Figs. 6, 7), which show that an avalanche of small particles on an undulated slope leads to a very regular and structured flow with important internal rotations and internal shearing.

3.3 Granular deposit

Positions and shapes of the granular deposits result from the avalanche kinematics and from the modes of energy dissipation before the mass stops. The eight quantitative descriptors of the dimensions of the granular deposit are provided in Fig. 11, for the simulations A1 to E1 (planar slope) and A2 to E2 (undulated slope). A number of interesting trends may be pointed out. Overall, whatever the size of the bricks, it seems that the slope waviness increases the fahrböschung
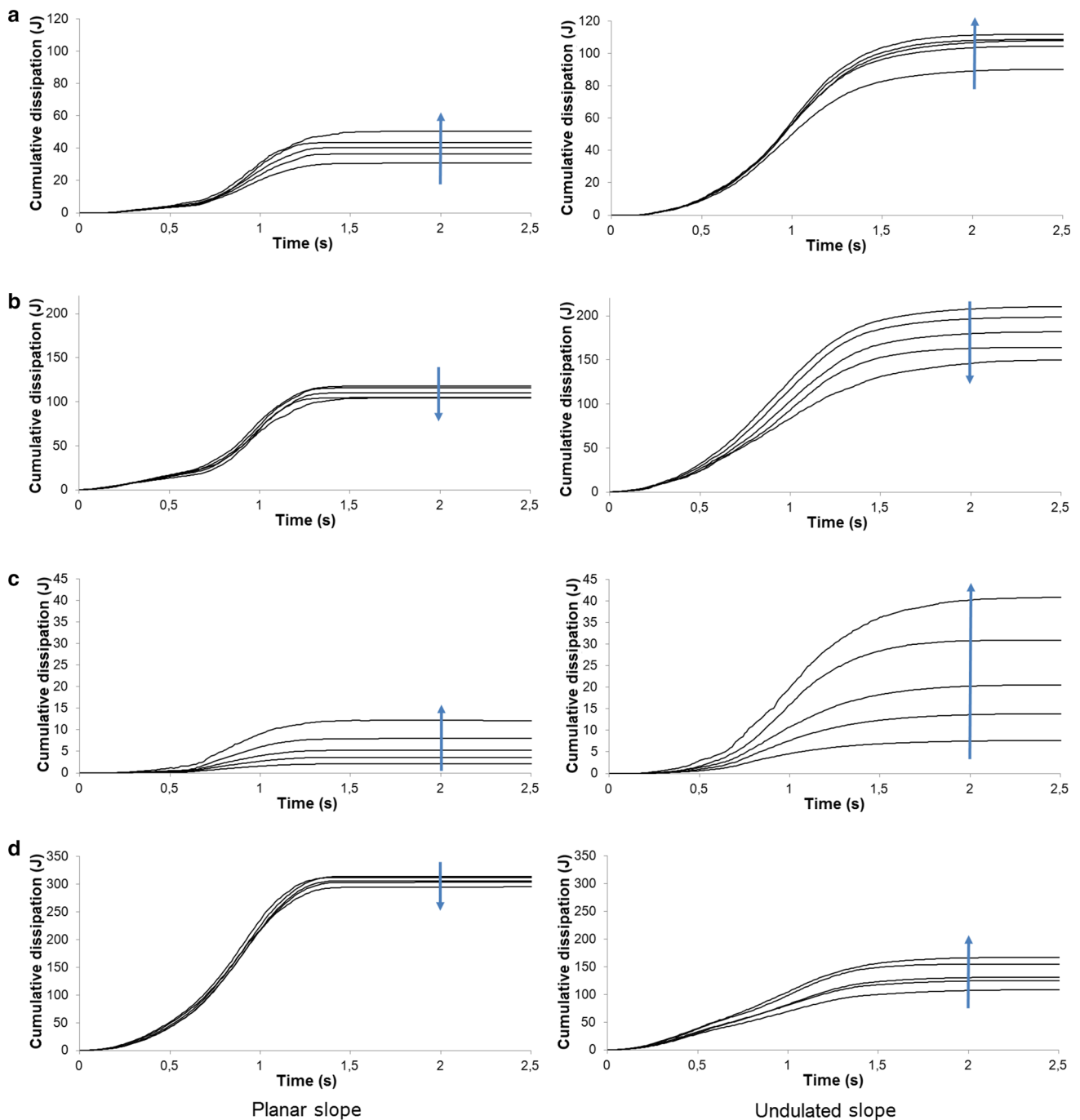
Fig. 10 Evolution in time of the four kinds of cumulative energy dissipations for various block sizes, on a planar and an undulated slope. The *blue arrows* point from the small particles (shape A) to the large ones (shape E). **a** Brick–brick collisional dissipation. **b** Brick–brick frictional dissipation. **c** Brick–support collisional dissipation. **d** Brick–support frictional dissipation (color figure online)

and the travel angles (by 4°–6°), and leads to deposits with smaller runout distance and length, and larger width and thickness. This is a direct consequence of the change in motion mode (from basal sliding to internal shearing) and in dissipative mode (from basal friction to internal dissipation) consecutively to the introduction of the waviness. On a planar slope, the size of the bricks has a limited influence on the characteristic dimensions of the deposit, as an

increase of the brick size only leads to a limited reduction of the horizontal dimensions of the deposit (length and width). In these cases (A1 to E1), avalanches are regular and governed mainly by basal frictional mechanisms regardless the sizes of the bricks. On an undulated slope, however, the influence of the brick sizes is much more important. Very small blocks (shape A) induce brick rotations, shearing in the granular mass, and an increase of shocks and
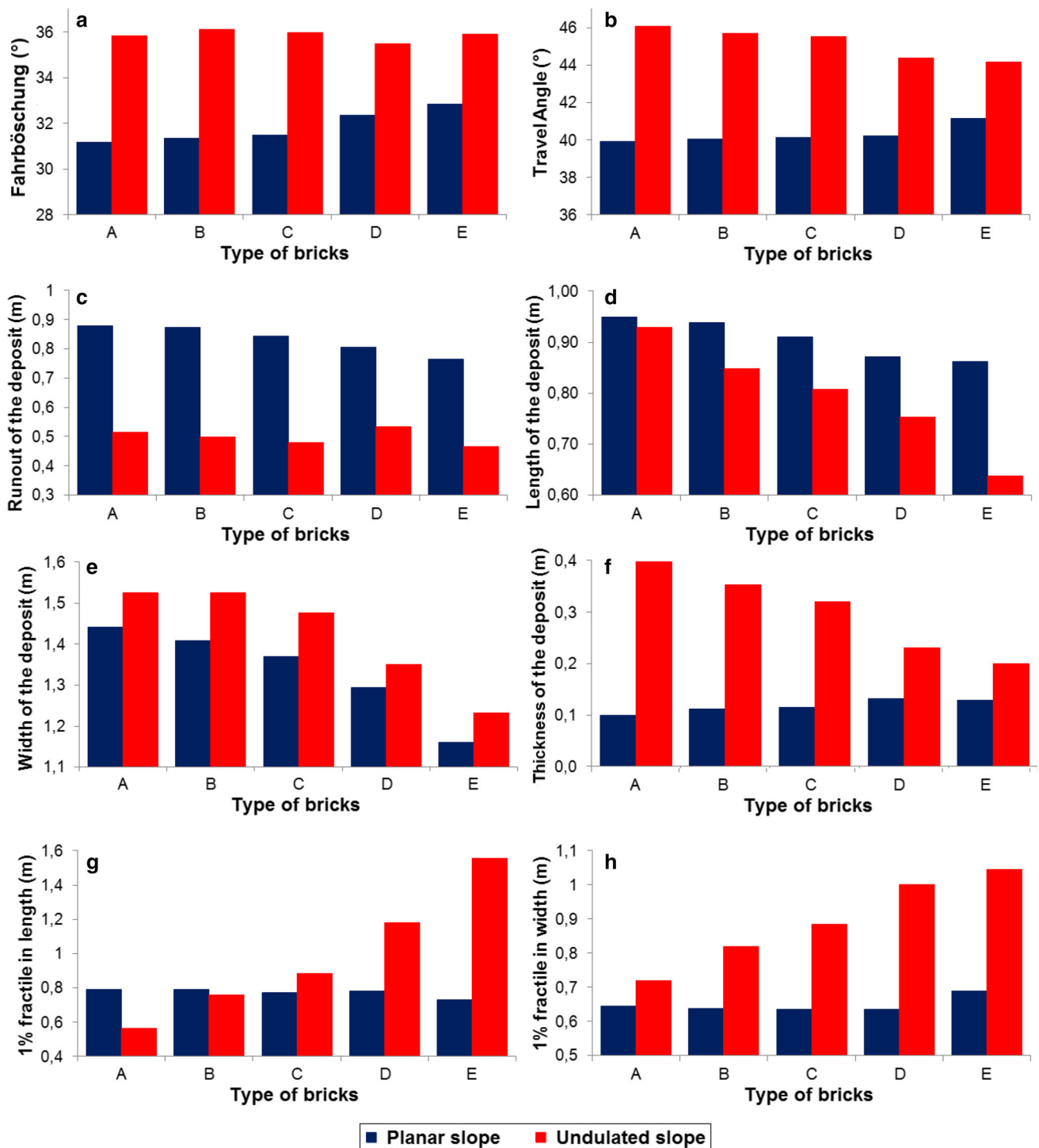
Fig. 11 Influence of the size of the particles on the fahrböschung (**a**), the travel angle (**b**), the runout (**c**), the dimensions of the deposit (**d**–**f**), and the 1 % fractiles (**g**, **h**), for a planar and an undulated slope

friction within the granular mass which will lead to more loose deposits with larger dimensions (length, width and thickness, see Fig. 11d–f) than with large blocks (shape E). Hence, there is an interaction between the particles and the ruggedness of the slope which leads to this size-dependence

that does not exist on a perfectly planar slope. Additional evidences of this interaction may be observed by paying attention to the 1 % fractiles in length and width (Fig. 11g, h). It is clear that, on a planar slope, the final dispersion of the bricks is not affected by their size since these frac-
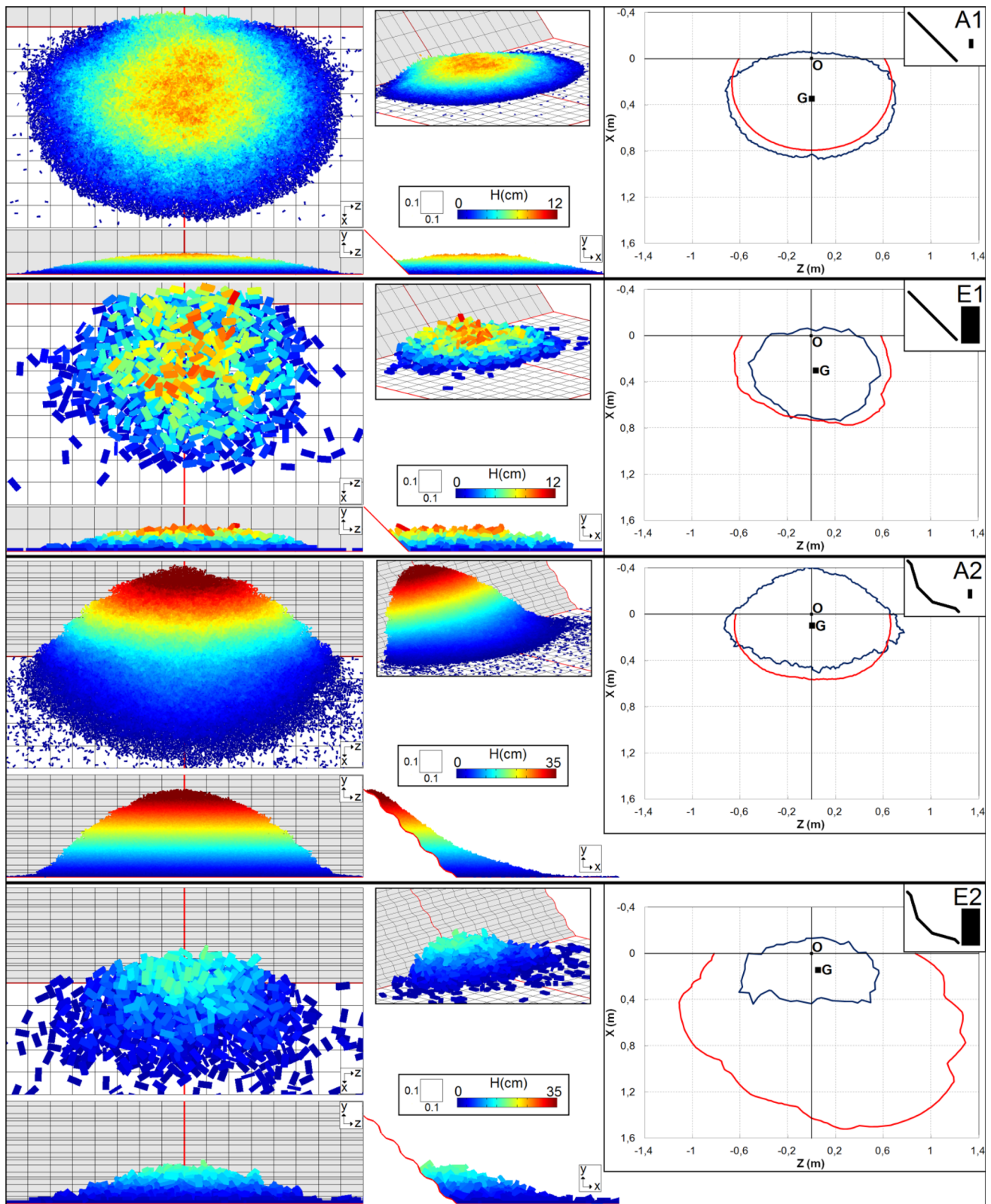
Fig. 12 Granular deposits obtained for simulations A1, E1, A2, and E2. *Left-hand column* top-view and front-view; *central column* side-view and perspective view; *right-hand column* top view of the outline of the deposit (*blue line*) and of the contour corresponding to the distance reached by 1 % of the particles in various directions (*red line*) (color figure online)

tiles are rather constant from simulations A1 to E1. On an undulated slope, however, the axial and lateral dispersions largely increase with the block size, which means that the waviness of the slope acts differently on small and on large bricks.

Figure 12 provides the layout of the granular deposits in the extreme cases (A and E), for both the planar and the undulated slopes, which confirm the previous results. For each case (e.g. A1), a top-view, and a front-view (left-hand column), together with a side-view and a perspective view (central column) of the final positions of the deposit are plotted. The color-scale corresponds to the elevation of the bricks. In these plots, the grey slope and the white horizontal plane help the reader to localize easily the change of gradient. Also, a top view of the outline of the deposit (in blue) and of the contour of the 1 %-fractiles (in red) is given in the right-hand column. The red curve is computed using a method similar to the one of the "1 % fractile in length" (as described in the previous paragraph), but in a finite set of horizontal and forward directions around the deposit. This method considers as a central point the intersection O between the main plane of symmetry of the apparatus (i.e. the plane Z=0) and the line of gradient change (Z-axis). Then it considers an arbitrary horizontal direction (making an angle θ with the X-axis, with $-\pi \leq \theta \leq \pi$), and determines the distance $d(\theta)$ for which there are 1 % of the particles located beyond a line perpendicular to the direction θ and located at a distance d of point O. This process is repeated for a large number of directions θ and finally provides the red curve plotted in Fig. 10. For $\theta = 0$, it is actually identical to the 1 %-fractile in length, described in the previous section. Hence, the red curve provides an estimate of the dispersion of the bricks in all the directions of space. The blue contour is directly obtained by the non-convex hull algorithm described in Mollon et al. [33], and provides an estimate of the contour of the connected deposit (ignoring separated blocks). The position of the centre of mass of the granular deposit is also shown in each case.

3.4 Reproducibility

In the results presented in this section and in the following ones, only one run of the model was performed in each case. This choice, mainly related to the high computational cost of each simulation, leaves open the question of the reproducibility of the results. Indeed, some randomness exists in the initial packing (since bricks are first positioned on a regular loose lattice but with random orientations), and this randomness might propagate to the results, at least to a certain extent. To address this problem, additional sets of simulations were performed. More specifically, five additional runs were launched for the cases B1 to E1 (the case A1 was ignored due its very high cost), and the variability of relevant outputs was computed in each set. Results are provided in Fig. 13a, which provides the average fahrböschung and travel angles for each set of simulations, as well as the related standard deviations. It is clear from these results that (1) a dispersion exists, but remains rather limited (less than 0.8° of standard deviation for the simulations E1 with 790 bricks), and that (2) this dispersion is much smaller when the number of bricks increases (i.e. when using smaller bricks). Fig. 13b, c shows that, although there is some limited visual differences between two deposits in the case E1, this difference is negligible when dealing with the case B1 with smaller particles. Based on these observations, we may infer that the results provided in this paper based on single runs can be trusted, even those involving large bricks.

4 Influence of the elongation of blocks

4.1 Avalanche kinematics and energy dissipations

In this section, we investigate the elongation of the blocks composing the released mass. A comparison between the shapes C (bricks, with a ratio between the largest and the smallest dimension close to 4) and F (cubes) provides clues
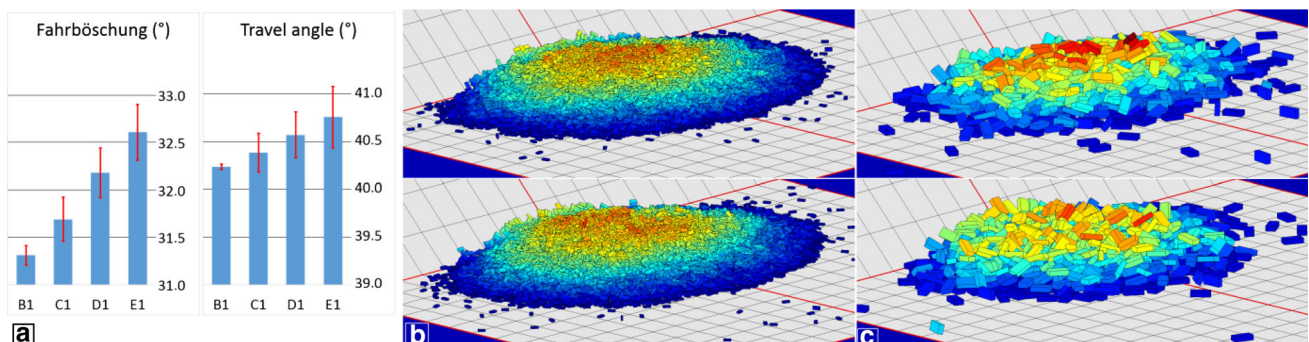

Fig. 13 Analysis of the reproducibility of discrete simulations. **a** Average values of fahrböschung and travel angles for the cases *B1* to *E1* (the *errors bars* correspond to one standard deviation); **b** two deposits obtained in the case *B1*; **c** two deposits obtained in the case *E1*
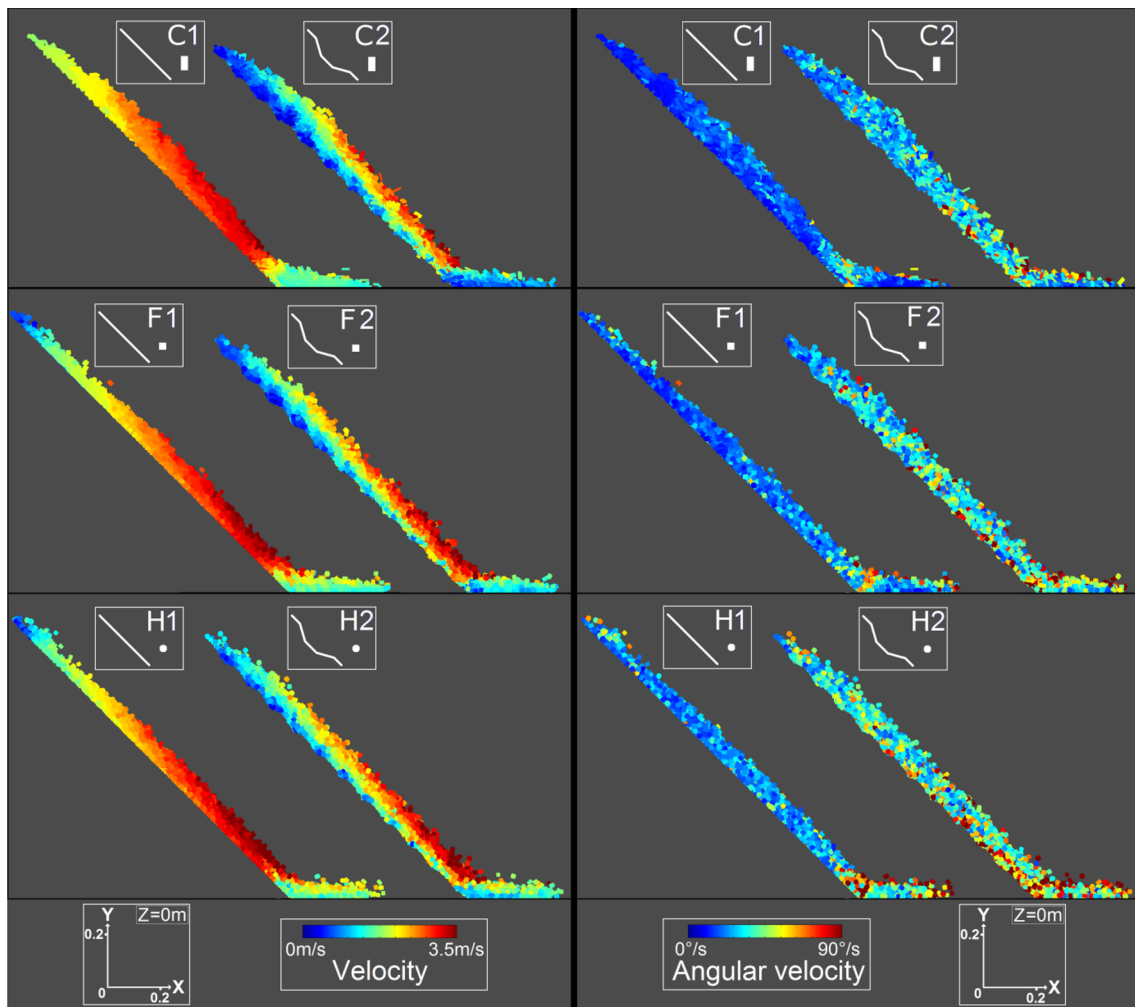
Fig. 14 Kinematics of the particles for blocks *C*, *F* and *H*, in longitudinal cross sections, when the fronts of the avalanches reach X = 0.4 m. *Left-hand panel* velocities; *right-hand panel* angular velocities

on the influence of the aspect ratio for a fixed volume. Indeed, shape C exhibits an aspect ratio which is absent from the cubic shape F. The velocity and angular velocity fields of these cases are provided in Fig. 14. As in Figs. 6 and 7, there is an important influence of the slope waviness on the kinematics. For cubes, a planar slope induces a slipping regime rather similar to that of bricks, with a velocity field homogeneous in vertical transverse cross-sections and with moderate block rotations. On the flat area, rotations of the cubes are less constrained. This leads to an increase of dispersion of particles. Slopes with undulations lead to internal shear in the flowing mass, with a marked vertical velocity gradient in the transverse cross-sections, and large block rotations in the whole mass. The first two rows of Fig. 14 show that there is no major difference between the kinematics of the avalanches of bricks and cubes, either for velocities or angular velocities.

The cumulative energy dissipations for the simulations C1, C2, F1, and F2 are recapitulated in Fig. 15. Just like in

Fig. 9, a difference is made between the dissipations occurring on the slope (zone 1), in the transition zone (zone 2), and on the horizontal plane (zone 3). On a planar slope, there is no major influence of the aspect ratio of the particles on the main dissipation patterns. The only noticeable influence is the fact that the collisional dissipation in the transition zone is larger for cubic particles (F) than for elongated ones (C). On an undulated slope, however, there is an important difference between cubic and elongated bricks in terms of dissipation patterns. Cubic blocks lead to a strong reduction of the frictional dissipations on the slope (zone 1), and to a limited increase of the collisional dissipation in the zone of transition (zone 2). Considering that the kinematics of the granular flow on the slope are rather similar from one case to another, this difference in behavior can be imputed to the aspect ratio of the bricks which allows for more frictional dissipation within the granular mass or with the support. As a result, only 4 % of the energy remains to be dissipated on
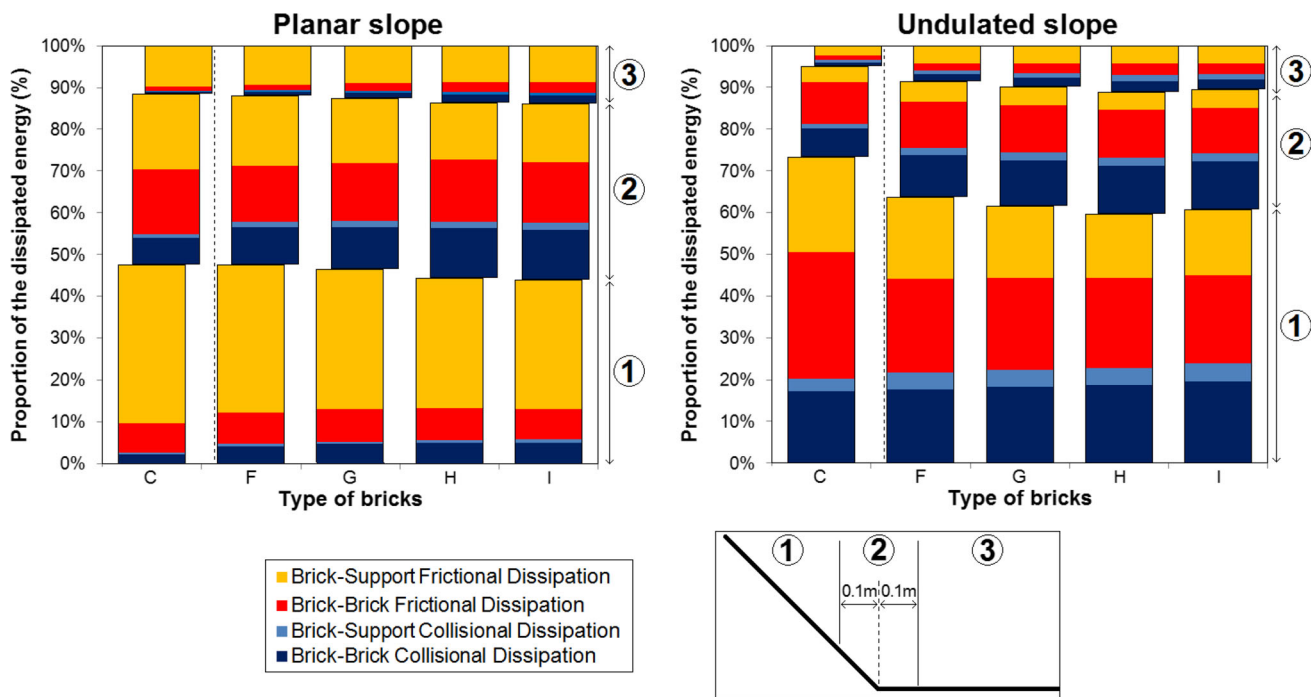
Fig. 15 Type and localization of the cumulative energy dissipations for various shapes of the blocks, on a planar and an undulated slope

the horizontal plane (zone 3) for the elongated bricks, while this proportion reaches 8 % for the cubic bricks.

4.2 Granular deposit

Figure 16 provides the values of the fahrböschung angle, the travel angle, the runout distance, the dimensions of the deposit and the dispersion fractiles, for the simulations C1, C2, F1 and F2. As clearly appears on this figure, the influence of the aspect ratio of the bricks on the position and dimensions of the deposit are rather limited in the case of a planar slope, and more noticeable in the case of an undulated slope.

In the case of a planar slope, the consideration of cubic particles (F) instead of elongated ones (C) leads to larger fahrböschung and travel angle, and to a smaller runout distance. In this case, the amount of energy dissipated for particles (C) on the slope and on the transition (Fig. 15) is higher in the same zones than for particles (F). From Fig. 14, it can be seen that bricks of type (C) tend to slip, whilst cubes of type (F) display a rolling ability on the horizontal plane. For the chosen set of mechanical parameters, on the flat zone, the energy dissipated by collisions during the rolling of particles (F) is higher than the energy dissipated by friction during the sliding of particles (C), and the runout distance of the latter particles is longer.

In the case of an undulated slope, a reverse trend is observed. Indeed, the energy dissipated by friction on the slope (Fig. 16) is much higher for the C-type particles, which rub against each other and with the support, than for the

cubes (F-type particles). The C-type particles have lost a lot of energy on the slope and thus have a lower runout distance. Hence, for a given set of the frictional and collisional parameters, a change in the particle shape may lead to opposite results in terms of avalanche propagation depending of the roughness of the slope. In contrast, the dimensions of the deposit follow the same trends on both slopes: cubic particles (case F) lead to a reduction of the length and of the thickness of the deposit and to an increase of its width, with respect to elongated ones (case C). The 1 % fractiles in length and width also show that cubic particles tend to get much more separated from the main avalanche and to increase the dispersion of the final deposits.

5 Influence of the angularity of blocks

5.1 Avalanche kinematics and energy dissipations

In this section, a comparison between the particles F, G, H and I is conducted in order to provide clues on the influence of their roundness (induced by the cutting parameter c, which increases from particle F to particle I, see Fig. 3). The last two rows of Fig. 14 provide the fields of velocities and rotational velocities of the particles, for the cases F1, H1, F2, and H2. These figures tend to demonstrate that with the adopted rounding procedure, the particle roundness has no major influence on the global kinematics of the avalanche. In the stop area, however, it appears that the amount of particle
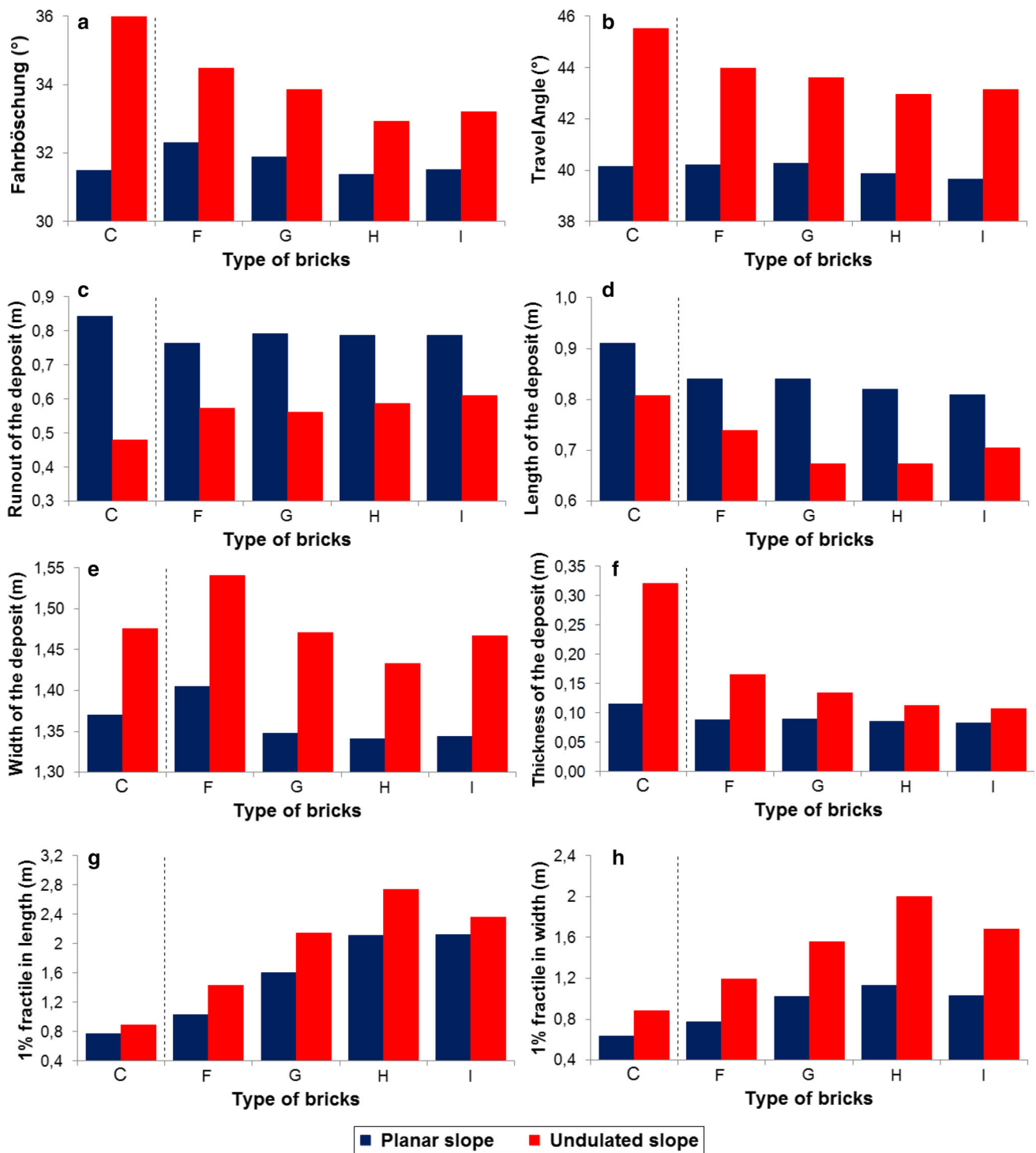
Fig. 16 Influence of particle shape on fahrböschung (**a**), travel angle (**b**), runout (**c**), dimensions of the deposit (**d–f**), and 1 % fractiles (**g**, **h**), for a planar and an undulated slope

rotations is slightly more important on the horizontal plane for the particles H than for the particles F, both for the planar and for the undulated slope. Besides, the rotations on the horizontal plane are larger for an undulated slope than for a planar slope. Apparently, the particles with cut corners have a

greater ability to roll on the horizontal plane after the gradient change, and this effect is increased by the macro-roughness of the slope.

The cumulative energy dissipations for the simulations F1 to I1, and F2 to I2 are recapitulated in Fig. 15, showing that the
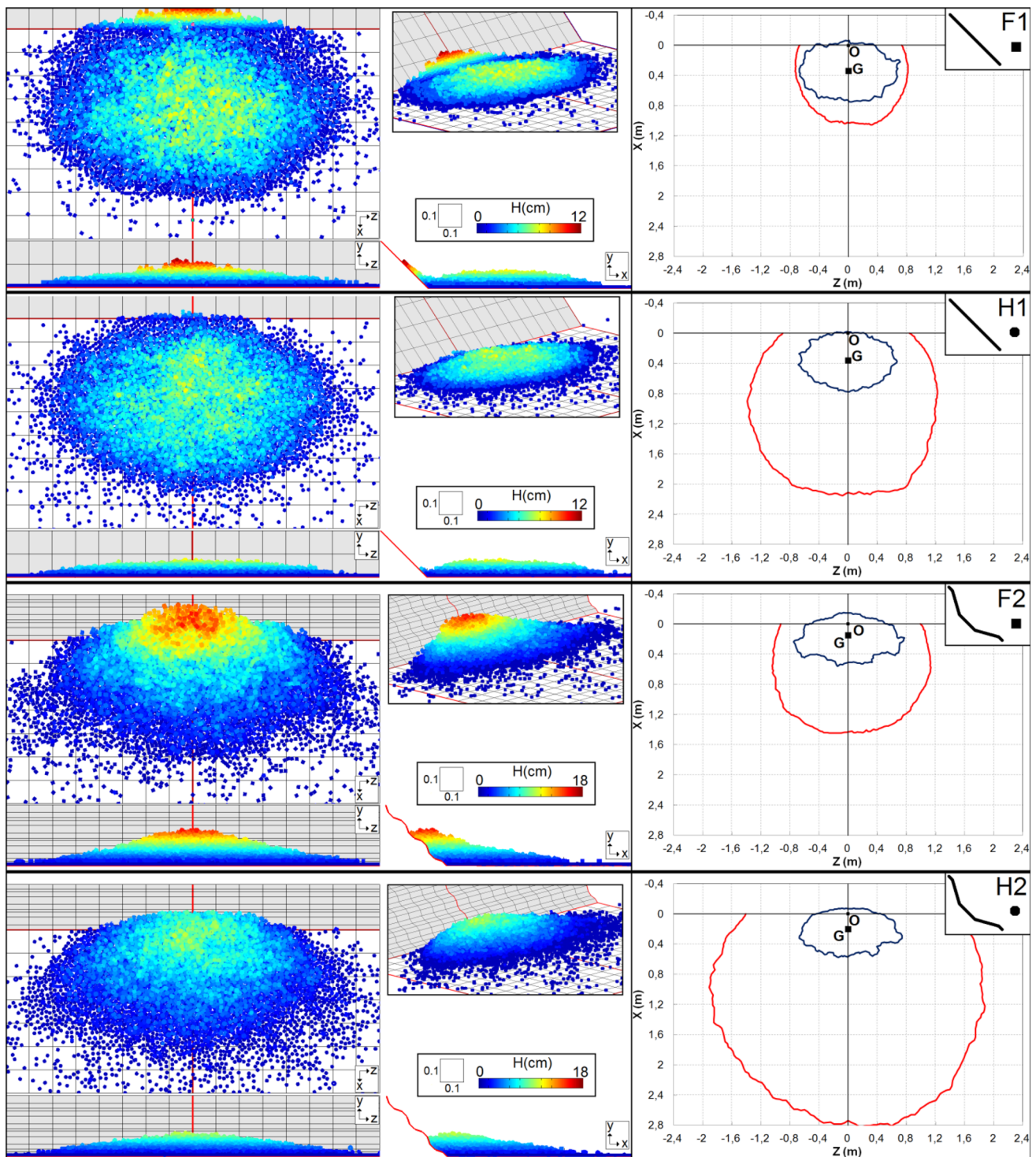
Fig. 17 Granular deposits obtained for simulations *F1*, *H1*, *F2*, and *H2*. *Left-hand column* top-view and front-view; *central column* side-view and perspective view; *right-hand column* top view of the outline of the deposit (*blue line*) and of the contour corresponding to the distance reached by 1 % of the particles in various directions (*red line*) (color figure online)

energy dissipations are not strongly influenced by the corner-cutting operation. For a planar slope, the most noticeable influence is related to an increase of the collisional dissipation on the slope and in the transition zone, correlated with an increase of the roundness. This increase in the collisional dissipation is probably related to a greater rolling ability of particles with cut corners (which increases the collisions in the area of disturbance of the flow), and is balanced by a slight

reduction of the basal frictional dissipation on the slope and in the transition zone (also probably related to rolling). On an undulated slope, the cases F2 to I2 show very similar patterns, except for the brick-base frictional dissipation on the slope, which is minimum for the case H2. Hence, in this simulation the percentage of energy dissipated on the horizontal plane is the largest (10 %).

5.2 Granular deposit

The observation of cases F to I in Fig. 16 shows that, on a planar slope, the influence of the angularity of the corners on the characteristics of the granular deposit (fahrböschung, travel angle, runout, length, width and thickness) is limited. In contrast, on an undulated slope, the cutting-length c has a strong influence on the final deposit. For the fahrböschung, the deposit length, the deposit width and the deposit thickness, some interesting trends appear: when increasing the cutting length c from 0 to 4 mm (i.e. in cases F2 to H2), we observe a decrease of the length, width and thickness of the deposit, which means that the deposit is more compact. The fahrböschung is also reduced. On the contrary, when increasing the cutting length c from 4 to 6 mm (cases H2 and I2), the deposit horizontal dimensions and the fahrböschung angle starts to reverse the trend and to increase again. Hence, among the four particles F to I, it appears that particle H leads to a maximum bulk density of the deposit. It seems logical to observe an increase of the final dispersion between cases F and H, since the fact of increasing the sphericity of the particles facilitates their ability to roll and to separate from the main avalanche. These results are further confirmed by the observations of the deposits provided in Fig. 17. However, it is unclear why this trend is reversed for particle I. Obviously, there are geometrical interactions between the flow regime, slope undulations, and particle shape, which remain beyond our understanding and deserve more investigation.

To illustrate this difficulty, a simple additional test was performed. The numerical model of the experimental device shown in Fig. 1 was used to release a single particle on a smooth slope, at the coordinates X = −1 m and Y = 1.03 m (in order to avoid any initial interpenetration with the slope) with a null initial velocity, and its trajectory on the slope and on the horizontal plane was monitored closely until its final stop. For a given particle shape, this operation was repeated 1,000 times with random initial orientations of the particles, in order to make statistics on the total distance of travel and on the X-coordinate of the final position of the particles. Indeed, these quantities may be regarded as "experimental" indicators of the rolling ability of a shape (although this is a numerical experiment in our framework). This test was repeated for numerous values of the corner-cutting parameter c, running from zero (perfect cube) to half the cube side-length L. The results of these simulations are provided in
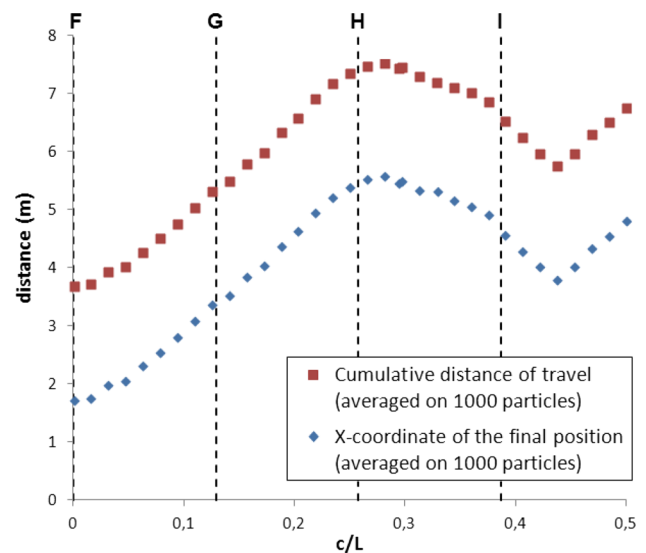

Fig. 18 Evolution of some indicators of the rolling ability of the particles as a function of the corner-cutting parameter c

Fig. 18, and demonstrate that the evolution of the rolling ability with the corner-cutting parameter c (scaled on the particle length L) is not monotonic. It increases from $c/L = 0$ to $c/L = 0.3$, then decreases until $c/L = 0.43$, and increases again until $c/L = 0.5$. This observation is in good agreement with the fact that particle H is that with the greatest rolling ability (among the particles F to I). It also reveals that the links between particle shape and rolling ability are very complex. Whether or not a single shape parameter (such as the corner-cutting distance used in the present paper, or any one of the numerous definitions of roundness and sphericity available in the literature) may be able to describe the rolling ability of a particle seems highly uncertain.

6 Discussion and conclusion

The results presented in the present paper reveal complex interactions between the properties of the blocks composing the avalanche (size, aspect ratio, roundness) and the geometry of the slope (waviness, sharp change of gradient). These interactions play a complicated role in the prediction of the final dimensions and position of the granular deposit and of the global dispersion of the blocks separated from the main avalanche. The major findings are recapitulated hereafter:

1. On a planar slope, the influence of the size of the blocks is rather limited. The avalanche is mostly in a translational regime (except in the transition zone, where it is quite disturbed by the change of gradient), the velocity field is constant in transverse cross-sections, the particle rotations are limited, and the packing density is constant

in the whole avalanche. Most of the kinetic energy is dissipated by friction at the base of the avalanche, between the bricks and the base. Considering larger bricks only slightly decreases the dimensions of the granular deposit and the bulk density of the avalanche, whilst it slightly increases the collisional energy dissipations. Whatever the size of the blocks, the final dispersion of the bricks is very limited, most of them remaining in the main deposit. These results seem in good agreement with experiments from the literature: Yang et al. [48], for example, report that cubic blocks, cobbles and gravels flow with the same velocity in a large flume with a smooth frictional substrate and a 45° slope. Larger bricks also tend to decrease slightly the mobility of the centre of mass of the avalanche. This is consistent with the experimental findings of Cagnoli and Romano [2], while Manzella and Labiouse [27] do not notice such a limited trend.

2. In contrast, on an undulated slope, there is a strong influence of the size of the blocks on the characteristics of the avalanche. Bricks with a size smaller than the characteristic dimensions of the slope waviness lead to a flow with strong internal shearing, with important vertical velocity gradient and particle rotations and a quite dense packing. In this case, velocities, angular velocities and local solid fractions are very well spatially correlated with the slope undulations, leading to periodic heterogeneities. As a result of the intense shearing in the granular mass, most of the energy is dissipated by friction between particles, which leads to a limited propagation of the granular mass, to a large percentage of particles stopping on the slope, and to a very limited final dispersion of the bricks. On the contrary, bricks with dimensions larger than those of the slope undulations lead to an unstructured and collisional flow, with important velocity gradients between neighboring particles, important rotations, and loose packing. These kinematics increase collisional dissipation and strongly reduce basal frictional dissipation, which leads to avalanches with a higher mobility and to the separation of a large portion of the particles from the main avalanche.

3. Considering cubic particles instead of elongated ones only slightly modifies the avalanche kinematics and the dissipative energy modes. For the chosen set of parameters, this implies a limited decrease of the avalanche mobility in the case of a planar slope, and an increase of the mobility in the case of a slope with undulations. Indeed, on a planar slope the larger rolling ability of the cubic particles induce larger rotations and a slightly larger collisional dissipation on the slope and in the transition zone. On the contrary, on an undulated slope, the combination of slope undulations and rolling ability of the cubic blocks leads to a strong disturbance of the flow in a manner similar to that observed with large bricks, makes the flow regime more collisional, and reduces the frictional dissipations on the slope and in the transition zone.

4. When compared to the cubic case, an increase in the roundness of the particles does not seem to have a major effect on the global kinematics of the avalanche, on the patterns of energy dissipations, and on the geometry and position of the granular deposit. However, it has a strong influence on the ability of the individual bricks to separate from the main avalanche, leading to a very important dispersion of the positions of the blocks at the end of the avalanche. This dispersion is related to the rolling ability of these shapes, which leads to important particle rotations after the transition zone. This behavior is particularly evident on an undulated slope, which strongly disturbs the flow even before the transition zone, and may lead to very wide final dispersions of the blocks.

On one hand, the results presented in this paper are in qualitative agreement with experimental observations described in the scientific literature. About the avalanche regime, Friedman et al. [13] state that "Often, a linear flow profile […] is observed. However, if the bottom surface on which the avalanche flows is smooth and has low friction, a plug flow develops". Manzella and Labiouse [26] state that "When […] the base friction increases, […] the centre of mass travels a shorter distance". When comparing gravel and bricks (i.e. two granular materials with different block size and shape) on a smooth slope, they also observe that "there is a certain similarity between the mechanism of propagation", which is also in agreement with the numerical results we propose. On the other hand, the fact that slope undulations induce strong differences (both in the avalanche regime and in the final deposit dispersion), depending on the size and shape of the blocks, still has to be validated experimentally. However, we can reasonably state from our results that, in the case of a slope exhibiting an important waviness (which is the case of many natural slopes), one might not be able to predict properly the final position of the deposit and the area impacted by individual blocks without considering important factors such as the sizes, aspect ratio, and roundness of the particles. Some trends were pointed out in the present paper, but they may not be generalized yet since only a certain type of slope roughness (longitudinal undulations) and a certain class of particles (bricks with planar and parallel faces, with or without cutting of the corners) were considered. In a future work, it seems necessary to move away from the experimental framework which was the initial basis of this numerical parametric study, and to investigate more general and realistic shapes. Moreover, to enhance our understanding of this complex type of granular flow, it might be interesting to pay attention to (1) a more appropriate modelling of the contact conditions in the

case of a real slope made of soft ground, (2) a more realistic roughness of the slope, and (3) the influence of the distribution of the sizes of the blocks, and of its evolution related to the block fragmentation process during the avalanche.

References

1. Banton, J., Villard, P., Jongmans, D., Scavia, C.: Two-dimensional discrete element models of debris avalanches: parameterisation and the reproducibility of experimental results. J. Geophys. Res. Earth Surf. **114** (2009). doi:10.1029/2008JF001161

2. Cagnoli, B., Romano, G.P.: Effects of flow volume and grain size on mobility of dry granular flows of angular rock fragments: a functional relationship of scaling parameters. J. Geophys. Res. Solid Earth **117**, B02207 (2012)

3. Cleary, P.W., Prakash, M.: Discrete-element modeling and smoothed particle hydrodynamics: potential in the environmental sciences. Philos. Trans. R. Soc. A Math. Phys. Eng. Sci. **362**, 2003–2030 (2004). doi:10.1098/rsta.2004.1428

4. Cuervo, S., Daudon, D., Richefeu, V., Villard, P., Lorentz, J.: Discrete element modeling of a rockfall in the south of the "Massif Central", France, IAEG XII Congress, Torino, Italia, pp. 15–19. Sept. (2014)

5. Cundall, P.A.: Formulation of a three-dimensional distinct element model—part I, a scheme to detect and represent contacts in a system composed of many polyhedral blocks. Int. J. Rock Mech. Min. Sci. **25**, 107–116 (1988)

6. Cundall, P.A., Strack, O.D.L.: A discrete numerical-model for granular assemblies. Geotechnique **29**(1), 47–65 (1979)

7. D'Addetta, G.A., Kun, F., Ramm, E.: On the application of a discrete model to the fracture process of cohesive granular materials. Granul. Matter **4**, 77–90 (2002)

8. Davies, T.R., McSaveney, M.J.: Runout of dry granular avalanches. Can. Geotech. J. **36**, 313–320 (1999). doi:10.1139/t98-108

9. Donze, F.V., Richefeu, V., Magnier, S.A.: Advances in discrete element method applied to soil, rock and concrete mechanics. State Art Geotech. Eng. Elect. J. Geotech. Eng. **44**, 1–44 (2009)

10. El Shamy, U., Gröger, T.: Micromechanical aspects of the shear strength of wet granular soils. Int. J. Numer. Anal. Meth. Geomech. **32**(14), 1763–1790 (2008)

11. Elghezal, L., Jamei, M., Georgopoulo, O.: DEM simulations of stiff and soft materials with crushable particles: an application of expanded perlite as a soft granular material. Granul. Matter **15**, 685–704 (2013). doi:10.1007/s10035-013-0406-z

12. Feng, Y.T., Owen, D.R.J.: A 2D polygon/polygon contact model: algorithmic aspects. Eng. Comput. **21**, 265–277 (2004)

13. Friedmann, S.J., Taberlet, N., Losert, W.: Rock-avalanche dynamics: insights from granular physics experiments. Int. J. Earth Sci. **95**, 911–919 (2006). doi:10.1007/s00531-006-0067-9

14. Ghaboussi, J., Barbosa, R.: Three-dimensional discrete element method for granular materials. Int. J. Numer. Anal. Methods Geomech. **14**, 451–472 (1990)

15. Goujon, C., Dalloz-Dubrujeaud, B., Thomas, N.: Bidisperse granular avalanches on inclined planes: a rich variety of behaviors. Eur. Phys. J. E **23**, 199–215 (2007). doi:10.1140/epje/i2006-10175-0

16. Han, K., Feng, Y., Owen, D.: Numerical simulations of irregular particle transport in turbulent flows using coupled lbm-dem. Comput. Meth. Eng. Sci. **18**(2), 87–100 (2007)

17. Hart, R., Cundall, P.A., Lemos, L.: Formulation of a three-dimensional distinct element model—part II, mechanical calculations for motion and interaction of a system composed of many polyhedralblocks. Int. J. Rock Mech. Min. Sci. **25**, 117–125 (1988)

18. Hogue, C.: Shape representation and contact detection for discrete element simulations of arbitrary geometries. Eng. Comput. **15**, 374–390 (1998)

19. Issa, J.A., Nelson, R.N.: Numerical analysis of micromechanical behaviour of granular materials. Eng. Comput. **9**, 211–223 (1992)

20. Iverson, R.M., Logan, M., Denlinger, R.P.: Granular avalanches across irregular three-dimensional terrain: 2. Experimental tests. J. Geophys. Res. **109**, F01015 (2004). doi:10.1029/2003JF000084

21. Jiang, M.J., Murakami, A.: Distinct element method analyses of idealized bonded-granulate cut slope. Granul. Matter **14**(3), 393–410 (2012)

22. Kumar, K., Soga, K., Delenne, J.Y.: Multi-scale modelling of granular avalanches. AIP Conf. Proc. **1542**, 1250 (2013)

23. Lin, X., Ng, T.T.: A three-dimensional discrete element model using arrays of ellipsoids. Geotechnique **47**, 319–329 (1997)

24. Luding, S.: About contact force-laws for cohesive friction al materials in 2D and 3D. In: Walzel, P., Linz, S., Krülle, C., Grochowski, R. (eds.) Behavior of Granular Media, Shaker Verlag, pp. 137–147. Band 9, Schriftenreihe Verfahrenstechnik, ISBN 3-8322-5524-9 (2006)

25. Mangeney-Castelnau, A., Vilotte, J.P., Bristeau, M.O., Perthame, B., Bouchut, F., Simeoni, C., Yerneni, S.: Numerical modeling of avalanches based on saint venant equations using a kinetic scheme. J. Geophys. Res. Solid Earth **108** (2003). doi:10.1029/2002JB002024

26. Manzella, I., Labiouse, V.: Flow experiments with gravel and blocks at small scale to investigate parameters and mechanisms involved in rock avalanches. Eng. Geol. Amst. **109**, 146–158 (2009). doi:10.1016/j.enggeo.2008.11.006

27. Manzella, I., Labiouse, V.: Empirical and analytical analyses of laboratory granular flows to investigate rock avalanche propagation. Landslides **10**, 23–36 (2013)

28. Matuttis, H.-G., Luding, S., Herrmann, H.J.: Discrete element simulations of dense packings and heaps made of spherical and non-spherical particles. Powder Technol. **109**, 278–292 (2000)

29. McDougall, S., Hungr, O.: A model for the analysis of rapid landslide motion across three-dimensional terrain. Can. Geotech. J. **41**, 1084–1097 (2004)

30. Mollon, G., Zhao, J.: Fourier–Voronoi-based generation of realistic samples for discrete modelling of granular materials. Granul. Matter **14**(5), 621–638 (2012). doi:10.1007/s10035-012-0356-x

31. Mollon, G., Zhao, J.: Generating realistic 3D sand particles using Fourier descriptors. Granul. Matter **15**(1), 95–108 (2013a). doi:10.1007/s10035-012-0380-x

32. Mollon, G., Zhao, J.: Characterization of fluctuations in granular hopper flow. Granul. Matter **15**(6), 827–840 (2013b)

33. Mollon, G., Richefeu, V., Villard, P., Daudon, D.: Numerical simulation of rock avalanches: influence of a local dissipative contact model on the collective behavior of granular material. J. Geophys. Res. **117**, F02036 (2012). doi:10.1029/2011JF002202

34. Mustoe, G.: A generalized formation of the discrete element method. Eng. Comput. **9**, 181–190 (1992)

35. Okura, Y., Kitahara, H., Sammori, T., Kawanami, A.: The effects of rockfall volume on runout distance. Eng. Geol. Amst. **58**, 109–124 (2000). doi:10.1016/S0013-7952(00)00049-1

36. Pirulli, M., Bristea, M.O., Mangeney, A., Scavia, C.: The effect of the earth pressure coefficients on the runout of granular material. Environ. Modell. Softw. **22**, 1437–1454 (2007). doi:10.1016/j.envsoft.2006.06.006

37. Pouliquen, O., Forterre, Y.: Friction law for dense granular flows: application to the motion of a mass down a rough inclined plane. J. Fluid Mech. **453**, 133–151 (2002). doi:10.1017/S0022112001006796

38. Richefeu, V., Youssoufi, M.E., Peyrous, M., Radjaï, F.: A model of capillary cohesion for numerical simulations of 3d polydisperse granular media. Int. J. Numer. Anal. Meth. Geomech. **32**(11), 1365–1383 (2007)

39. Richefeu, V., Mollon, G., Daudon, D., Villard, P.: Dissipative contacts and realistic block shapes for modeling rock avalanches. Eng. Geol. **149–150**, 78–92 (2012). doi:10.1016/j.enggeo.2012.07.021

40. Savage, S.B., Hutter, K.: The motion of a finite mass of granular material down a rough incline. J. Fluid Mech. **199**, 177–215 (1989). doi:10.1017/S0022112089000340

41. Scholtès, L., Chareyre, B., Nicot, F., Darve, F.: Micromechanics of granular materials with capillary effects. Int. J. Eng. Sci. **47**(1), 64–75 (2009)

42. Shi, G., Goodman, R.E.: Discontinuous deformation analysis—a new method for computing stress, strain, and sliding of block systems. In: Cundall, P.A., Sterling, R.L., Starfield, A.M. (eds.) Key questions in mechanicsn Proceedings of the 29th US symposium on rock mechanics, University of Minnesota, June 13–15, 1988, Balkema, pp. 381–393 (1988)

43. Taboada, A., Estrada, N.: Rock-and-soil avalanches: theory and simulation. J. Geophys. Res. **114**, F03004 (2009). doi:10.1029/2008JF001072

44. Ting, J.M., Khwaja, M., Meachum, L.R., Rowell, J.D.: An ellipse-based discrete element model for granular materials. Int. J. Anal. Numer. Methods Geomech. **17**, 603–623 (1993)

45. Tommasi, P., Campedel, P., Consorti, C., Ribacchi, R.: A discontinuous approach to the numerical modelling of rock avalanches. Rock Mech. Rock Eng. **41**(1), 37–58 (2008)

46. Tsoungui, O., Vallet, D., Charmet, J.C.: Numerical model of crushing of grains inside two-dimensional granular materials. Powder Technol. **105**, 190–198 (1999)

47. Valentino, R., Barla, G., Montrasio, L.: Experimental analysis and micromechanical modelling of dry granular flow and impacts in laboratory flume tests. Rock Mech. Rock Eng. **4**(1), 153–177 (2008)

48. Yang, Q., Cai, F., ugai, K., Yamada, M., Su, Z., Ahmed, A., Huang, R., Xu, Q.: Some factors affecting mass-front velocity of rapid dry granular flows in a large flume. Eng. Geol. **122**(2011), 249–260 (2011)

49. Zeghal, M., El Shamy, U.: Liquefaction of saturated loose and cemented granular soils. Powder Technol. Discrete Elem. Modell. Fluid. Beds **184**(2), 254–265 (2008). (Special Issue: Dedicated to Professor Yutaka Tsuji)

50. Zhou, G.G.D., Sun, Q.C.: Three-dimensional numerical study on flow regimes of dry granular flows by DEM. Powder Technol. **239**, 115–127 (2013)